Article

Cell Metabolism

A Conserved Mito-Cytosolic Translational Balance Links Two Longevity Pathways

Graphical Abstract

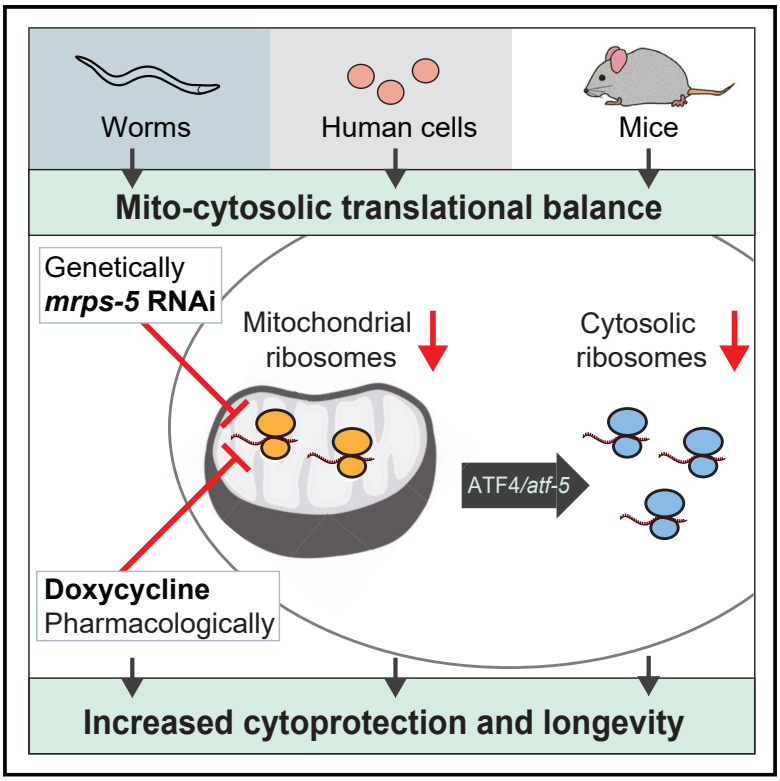

Highlights

- Mitochondrial and cytosolic ribosomal proteins are balanced with a natural ratio
- Blocking mitochondrial ribosomes in worms and mice reduces cytosolic translation
- Translational balance is ATF4/*atf-5*-dependent and conserved in human cells
- *atf-5*-induced translational repression is independent from mitochondrial bioenergetics

Authors

Marte Molenaars,
Georges E. Janssens,
Evan G. Williams, ..., Ruedi Aebersold,
Alyson W. MacInnes,
Riekelt H. Houtkooper

Correspondence

r.h.houtkooper@amsterdamumc.nl

In Brief

Molenaars, Janssens, and colleagues report on a natural balance between cytosolic and mitochondrial ribosomal proteins, driven by an active link between two longevity pathways. They demonstrate that the inhibition of mitochondrial translation regulates cytosolic translation via the transcription factor *Atf4/atf-5*, a phenomenon conserved in worms, human cells, and *in vivo* in mice.

Molenaars et al., 2020, Cell Metabolism *31*, 1–15
March 3, 2020
https://doi.org/10.1016/j.cmet.2020.01.011

CellPress

Please cite this article in press as: Molenaars et al., A Conserved Mito-Cytosolic Translational Balance Links Two Longevity Pathways, Cell Metabolism (2020), https://doi.org/10.1016/j.cmet.2020.01.011

Cell Metabolism
Article

A Conserved Mito-Cytosolic Translational Balance Links Two Longevity Pathways

Marte Molenaars,[1,11] Georges E. Janssens,[1,11] Evan G. Williams,[2] Aldo Jongejan,[3] Jiayi Lan,[2] Sylvie Rabot,[4] Fatima Joly,[4] Perry D. Moerland,[3] Bauke V. Schomakers,[1,5] Marco Lezzerini,[1] Yasmine J. Liu,[1] Mark A. McCormick,[6,7] Brian K. Kennedy,[8,9] Michel van Weeghel,[1,5] Antoine H.C. van Kampen,[3] Ruedi Aebersold,[2,10] Alyson W. MacInnes,[1] and Riekelt H. Houtkooper[1,12,*]

[1]Laboratory Genetic Metabolic Diseases, Amsterdam UMC, University of Amsterdam, Amsterdam Gastroenterology and Metabolism, Amsterdam Cardiovascular Sciences, Amsterdam, the Netherlands
[2]Institute of Molecular Systems Biology, ETH Zurich, Zürich, Switzerland
[3]Bioinformatics Laboratory, Amsterdam UMC, University of Amsterdam, Amsterdam, the Netherlands
[4]Micalis Institute, INRA, AgroParisTech, Université Paris-Saclay, Jouy-en-Josas, France
[5]Core Facility Metabolomics, Amsterdam UMC, University of Amsterdam, Amsterdam, the Netherlands
[6]Department of Biochemistry and Molecular Biology, School of Medicine, University of New Mexico Health Sciences Center, Albuquerque, NM, USA
[7]Autophagy, Inflammation, and Metabolism Center of Biological Research Excellence, University of New Mexico Health Sciences Center, Albuquerque, NM, USA
[8]Buck Institute for Research on Aging, Novato, CA, USA
[9]Departments of Biochemistry and Physiology, Yong Loo Lin School of Medicine, National University of Singapore, Singapore, Singapore
[10]Faculty of Science, University of Zürich, Switzerland
[11]These authors contributed equally
[12]Lead Contact
*Correspondence: r.h.houtkooper@amsterdamumc.nl
https://doi.org/10.1016/j.cmet.2020.01.011

SUMMARY

Slowing down translation in either the cytosol or the mitochondria is a conserved longevity mechanism. Here, we found a non-interventional natural correlation of mitochondrial and cytosolic ribosomal proteins (RPs) in mouse population genetics, suggesting a translational balance. Inhibiting mitochondrial translation in *C. elegans* through *mrps-5* RNAi repressed cytosolic translation. Transcriptomics integrated with proteomics revealed that this inhibition specifically reduced translational efficiency of mRNAs required in growth pathways while increasing stress response mRNAs. The repression of cytosolic translation and extension of lifespan from *mrps-5* RNAi were dependent on *atf-5*/ATF4 and independent from metabolic phenotypes. We found the translational balance to be conserved in mammalian cells upon inhibiting mitochondrial translation pharmacologically with doxycycline. Lastly, extending this *in vivo*, doxycycline repressed cytosolic translation in the livers of germ-free mice. These data demonstrate that inhibiting mitochondrial translation initiates an *atf-5*/ATF4-dependent cascade leading to coordinated repression of cytosolic translation, which could be targeted to promote longevity.

INTRODUCTION

The translation of mRNA into protein is essential for the growth and survival of every cell. Translation is carried out by small and large ribosomal subunits associating with mRNA assisted by eukaryotic initiation factors (eIFs) and elongation factors (eEFs) to ensure its speed and accuracy. The biogenesis of

Context and Significance

Aging has long been considered a passive process. However, research has established important, active roles for metabolic pathways in aging and age-related diseases. For instance, slowing down the production of new proteins generated by the ribosomes in the cytosol is known to extend lifespan in model organisms. Mitochondria exhibit their own distinct ribosomes, which also extend lifespan when slowed down. The current study found that these two longevity pathways are linked, and mitochondrial and cytosolic ribosomes maintain stoichiometric balance. The authors found that when mitochondrial translation is inhibited either genetically or pharmacologically, cytosolic translation is also inhibited, a phenomenon conserved from worms to mammals. The mito-cytosolic translational balance identified in this study can be used to promote healthy aging.

ribosomes coupled to mRNA translation has been estimated to be the most energy-consuming process in the cell (Buttgereit and Brand, 1995; Lane and Martin, 2010; Wieser and Krumschnabel, 2001). Slowing down translation by reducing expression of ribosomal proteins (RPs), eIFs/eEFs, or ribosomal RNA (rRNA) results in lifespan extension in yeast, worms, and flies (Chiocchetti et al., 2007; Hansen et al., 2007; Pan et al., 2007). This suggests a universal mechanism of lifespan extension lies in conserving the energy normally expended on cytosolic mRNA translation.

Distinct from the ribosomes in the cytosol, ribosomes that reside in the mitochondria are dedicated to translating the mRNAs encoded by the mitochondrial DNA. Because of the endosymbiotic "bacterial" origin of the mitochondria, mitochondrial ribosomes are structurally more similar to bacterial ribosomes than to their cytosolic counterparts (Greber et al., 2014, 2015; Smits et al., 2007). Compared to cytosolic ribosomes, mitochondrial ribosomes only need to translate a relatively small set of 13 mRNAs coding for subunits of the oxidative phosphorylation (OXPHOS) complexes that are required for the generation of ATP. Remarkably, slowing down mitochondrial translation also extends lifespan (Houtkooper et al., 2013). Inhibiting mitochondrial translation genetically (e.g., by knocking down mitochondrial ribosomal genes) or pharmacologically (e.g., by using the antibiotic doxycycline) results in mitonuclear protein imbalance and activates the mitochondrial unfolded protein response (UPR^{mt}) in a process conserved from worms to mammals (Houtkooper et al., 2013; Jovaisaite and Auwerx, 2015). The UPR^{mt} includes the upregulated expression of cytoprotective genes, such as those coding for mitochondrial heat shock proteins 6 and 60 (*hsp-6* and *hsp-60*) (Haynes and Ron, 2010). Other aspects of this response initiated by stressed mitochondria are mediated by *Atf4 (C. elegans atf-5*) (Quirós et al., 2017), a cyclic AMP-dependent transcription factor that has been implicated in a variety of mouse longevity models (Li et al., 2014).

Although mitochondrial and cytosolic ribosomes are separate translational apparatuses, they depend on each other to coordinate mitochondrial function, in particular the synthesis of OXPHOS proteins. A regulatory signaling route from cytosolic translation to mitochondrial translation has been reported in yeast and is allegedly strictly unidirectional (Couvillion et al., 2016). However, because mitochondria produce cellular energy and translation in the cytosol is a vast consumer of this energy, we hypothesized that there may be bidirectional translational control.

Here, we investigated the correlation of abundances between mitochondrial and cytosolic RPs in the BXD genetic reference population of mice (Wang et al., 2016). To address the direct link between mitochondrial and cytosolic translation, we have used a worm model of genetically impaired mitochondrial translation (RNAi-mediated knockdown of *mrps-5*) and observed a decrease in cytosolic translation using polysome profiling. By integrating "omics" data on three levels of biology (transcriptomics of the whole worm, transcriptomics of the polysomal fraction of the worm [highly translated transcripts], and proteomics), we explored an integrated, system-level view of the molecular changes induced via knockdown of mitochondrial translation that result in longevity. To show that key elements of this process are evolutionarily conserved, we used the antibiotic doxycycline as a means to reduce mitochondrial translation in human K562 cells and *in vivo* in mice. The findings of this study indicate that a bidirectional regulation exists between the two translation machineries across species, regulating longevity.

RESULTS

Mitochondrial and Cytosolic Ribosomal Proteins Co-correlate in a Natural Population of Mice

The degree to which the mitochondrial and cytosolic ribosomes longevity pathways regulate one another is not well understood (illustrated in Figure 1A). However, it seems likely that cross-communication between these systems exists, allowing for the suppression of translation should either machinery become compromised in order to maintain equal rates of production. Therefore, one would expect the natural abundances of these two translation machineries to match one another in varying cell types, tissues, or individuals in a population. In order to evaluate the possible natural balance in abundances that occurs between elements of the mitochondrial and cytosolic translational machinery, we turned to the population of BXD mouse strains. These segregate for around 5 million sequence variants, which in turn lead to expression variation in the transcriptome and proteome with a complexity similar to human populations (Wang et al., 2016). To resolve the relationships between the mitochondrial and cytosolic translation machineries in the mouse BXD liver proteome data, we reconstructed the protein correlation network between the individual elements of these protein complexes (Figure 1B; Table S1). Using a fairly permissive cutoff criteria ($p < 5e{-}4$), we observed robust correlations within both the subunits of the cytoribosome and mitoribosome ($p < 1e{-}4$, $p = 0.014$, respectively), and importantly, strong interactions *between* these translation machineries ($p < 1e{-}4$). To confirm the robustness of this observation, we turned to a separate mouse study (Williams et al., 2018) examining the regulation of proteins across eight BXD strains and across four different tissues (Figure 1B). Indeed, we found RPs from both ribosome types clustered and co-varied as observed in the liver-specific data, suggesting a general mechanism is in place ensuring mito-cytosolic translational balance. As expected, taking the average abundance of either cytosolic or mitochondrial RPs for each BXD strain showed variation to exist within each ribosome type (Figure 1C), and evaluating average mitochondrial ribosome abundances in relation to the average levels of cytosolic ribosomes within individual BXD strains confirmed the strong correlation between these two translation machineries (Pearson $R = 0.60$, $p < 0.05$) (Figure 1D). Taken together, these findings demonstrate that mitochondrial ribosome and cytosolic ribosome abundances are tightly regulated to stay in natural stoichiometric ratios.

Previous work in yeast has suggested a unidirectional relationship between these two translation machineries, whereby disruption of cytosolic ribosomes can concomitantly reduce abundances of mitochondrial ribosomes but not the reverse (Couvillion et al., 2016). To test the hypothesis that regulation could also occur in the opposite direction, namely mitochondrial ribosomes influencing the cytosolic ribosomes, we turned to *C. elegans* with reduced levels of mitochondrial small ribosomal protein 5 (*mrps-5*). In addition to inhibiting mitochondrial

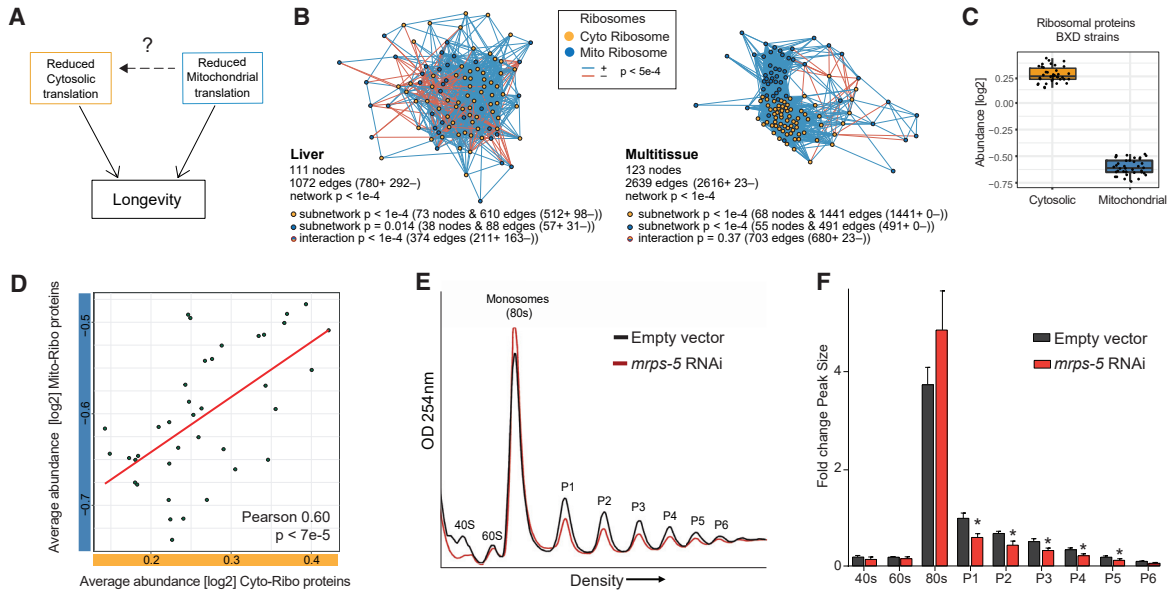

Figure 1. A Conserved Mito-Cytosolic Translational Balance in Mice and Worms

(A) Model showing possible links between two branches of translation regulation in lifespan control; cytosolic (yellow) and mitochondrial (blue).

(B) Correlation networks in BXD mice show strong relationships between mitochondrial and cytosolic ribosomal protein levels both in liver (left) and across multiple tissues (right), suggesting that the subunits within ribosomes and across ribosomes are co-regulated. Both networks show enriched connectivity. Liver: 73 nodes for the cytoribosome subnetwork have 610 edges ($p < 1e{-}4$, 512 are positively correlated), 38 nodes for the mitoribosome subnetwork have 88 edges ($p = 0.014$, 57 are positively correlated), 374 nodes are involved in the interaction between mitoribosome and cytoribosome subnetworks ($p < 1e{-}4$, 211 are positively correlated). Multitissue: 68 nodes for the cytoribosome subnetwork have 1,441 edges ($p < 1e{-}4$, 1,441 are positively correlated), 55 nodes for the mitoribosome subnetwork have 491 edges ($p < 1e{-}4$, 491 are positively correlated), 703 nodes are involved in the interaction between mitoribosome and cytoribosome subnetworks ($p < 1e{-}4$, 680 are positively correlated). For significance testing, 10,000 random networks were permuted using the same input data and gene set size for each dataset and subset with gene sets of the same size selected at random out of the full proteomic datasets. A reported $p < 1e{-}4$ means that none of the 10,000 random networks were as significant as the selected ribosome gene sets taken from literature.

(C) BXD mouse strains showing natural variation in cytosolic (yellow) or mitochondrial (blue) ribosome abundances in liver proteome. Each dot represents one BXD strain's average abundance of either the cytosolic or mitochondrial ribosomes.

(D) Averaged abundances from mitochondrial and cytosolic ribosomes in the BXD liver proteome (from C) show correlation between mitochondrial and cytosolic abundances (Pearson 0.60, $p < 7e{-}5$).

(E) Representative polysome profiles showing decreased cytosolic polysome abundances in worms with impaired mitochondrial ribosomal biogenesis (*mrps-5* RNAi). Lysate is normalized to protein levels. The subunits (40S and 60S), monosomal peak (80S), and polysomal peak numbers are indicated (P1–P6).

(F) Quantification of polysome peak sizes of representative experiment with n = 4 per condition normalized to P1 peak of empty vector control worms. Error bars represent mean ± SD and significance was tested with Student's t test, and p values were adjusted to correct for multiple testing using the Holm-Šídák method, with $\alpha = 0.05$.

See also Figure S1 and Table S1.

translation, RNAi of *mrps-5* induces the UPR^{mt}, alters mitochondrial function, prevents aging-associated functional decline, and extends lifespan in *C. elegans* (Houtkooper et al., 2013). To assess the status of cytosolic translation in *mrps-5* worms, we used a polysome profiling technique whereby free ribosomal subunits, monosomes (mRNA with one ribosome associated), and polysomes (mRNA with two or more ribosomes associated), are separated over a sucrose density gradient and quantified by optical density. Remarkably, in *mrps*-5 RNAi treated worms, we observed a shift from polysomes to monosomes, suggesting that more cytosolic mRNAs are being translated by a single ribosome instead of multiple following mitochondrial translation inhibition (Figure 1E). Indeed, quantification of the profiles confirmed a significant reduction of polysomal peaks in the *mrps-5* worms, revealing a suppression of cytosolic translation occurring in worms with an impaired mitochondrial ribosome (Figure 1F). To establish if this is a universal effect caused by mitochondrial disturbances, we performed polysome profiling in worms treated with either *eat-3* or *fzo-1* RNAi, which do not target the mito-ribosome but do target mitochondrial fusion. Both these conditions activated the UPR^{mt} and decreased respiration (Liu et al., 2019) but did not repress cytosolic translation (Figures S1A and S1B).

Together, these observations demonstrate that in addition to the established communication from the cytosol and mitochondria, a second and novel relationship exists whereby the mitochondrial ribosome communicates with the cytosolic translational machinery.

mrps-5 RNAi-Treated Worms Display Reduced Translational Efficiency of Cytosolic Ribosomal Proteins

Having observed a decrease in global translation occurring in *mrps-5* RNAi-treated worms, we next inquired as to what genes are specifically repressed at the translational level, i.e., in our polysomal fractions. In order to do so, we generated RNA sequencing (RNA-seq) libraries of polysomal and monosomal

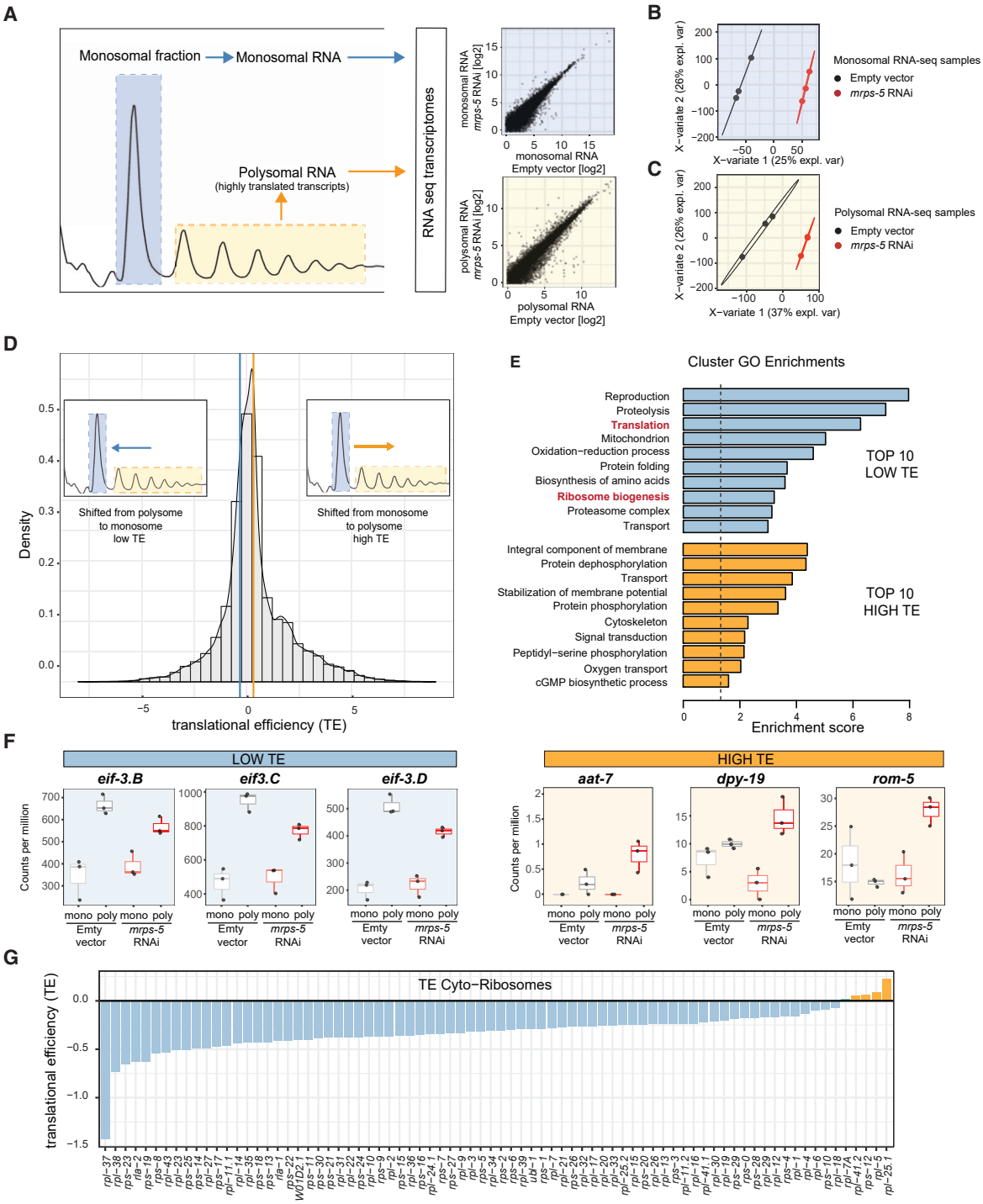

Figure 2. *mrps-5* RNAi-Treated Worms Show Reduced Translational Efficiencies for Cytosolic Ribosomal Genes

(A) Schematic showing RNA isolated from polysome profiles, from highly translated fractions (yellow, polysome) and lesser translated fractions (blue, monosome). RNA-seq transcriptomics was performed on polysomal and monosomal fractions for *mrps-5* RNAi and control worms. Transcripts (log2 transformed normalized counts) are depicted (scatterplots). Biological triplicates were used for each condition.

(B and C) Partial least-squares discriminant analysis (PLS-DA) for monosomal (B) and polysomal (C) RNA libraries showing clear distinction between *mrps-5* RNAi and control samples. Analysis was used to derive VIP scores for genes contributing most to the group separation.

(D) Translational efficiencies (TEs) of transcripts, defined as the log2 ratio of polysomal versus monosomal differences between *mrps-5* RNAi and control gene expression, shows shifts in transcripts from either the monosome to the polysome (high TE, yellow) or the polysome to the monosome (low TE, blue). Insets schematically depict the shifts observed in the histogram. Cutoff lines and VIP scores were used to remove noise for calculating enrichment of biological processes in low or high TE mRNAs.

(legend continued on next page)

fractions of RNA from *mrps-5* and control worms for comparison. The RNA-seq transcriptomes provided reliable quantification of over 16,000 genes covering the majority of the worm genome, allowing for a global description of the differences existing between monosome and polysomal RNA fractions (Figure 2A; Table S2).

To capture the broad-spectrum set of changes that discriminate between *mrps-5* and control worms at either the monosomal or polysomal levels, we performed a partial least-squares discriminant analysis (PLS-DA) on the samples for each condition. We found this to effectively distinguish *mrps-5* from control worms (Figures 2B and 2C; Table S2). Notably, this method is effective as a feature selector in addition to a sample classifier and is therefore useful in that it provides a variable of importance (VIP) ranking for each gene corresponding to its contribution in group discrimination (Boulesteix and Strimmer, 2007). This VIP score correlates highly to traditional p value ranking (Figures S2A and S2B) though it allows for a broader set of changes to be considered, which is more representative of the multifactorial nature of complex biological phenotypes. To explore the biological differences between groups in this way, we assessed genes with a high VIP score (>1) and turned to the Database for Annotation, Visualization and Integrated Discovery (DAVID) bioinformatics resource (Huang da et al., 2009). DAVID analysis clusters enrichments in Gene Ontology (GO) and various pathway databases, including Kyoto Encyclopedia of Genes and Genomes (KEGG) and Interprot, based on recurrence and similarities of genes in enriched pathways. With this method, we noted a wide variety of changes between *mrps-5* RNAi and control worms (Table S2). For instance, changes in the *mrps-5* monosomal RNA included an upregulation of RNAs coding for mitochondrial transit peptides (e.g., genes *asg-2*, *atad-3*, *cyc-2.1*) and a suppression of RNAs important for cuticle formation and other developmental pathways (e.g., genes *bli-6*, *col-81*, *rol-1*). A parallel upregulation of RNAs coding for mitochondrial transit peptides in the polysomes of *mrps-5* (e.g., genes *aco-2*, *coq-8*, *phb-2*) was also found along with a similar suppression of RNAs coding for proteins important for reproduction and growth (e.g., genes *acn-1*, *epi-1*, *ptr-4*) (Table S2).

In order to identify what transcripts were shifting from polysomal to monosomal fractions, and vice versa, we calculated the translational efficiency (TE) of each gene. The TE is defined as the ratio of the polysomal RNA to the monosomal RNA fraction for *mrps-5* RNAi relative to control worm. Upon log2 transformation, a positive TE value then corresponds to transcripts that shift from the monosome to the polysome in *mrps-5* RNAi relative to control, whereas negative TE values correspond to a shift in the opposite direction (Figure 2D; Table S2). Setting a low minimal fold-change TE cutoff of 1.25 with a significant VIP score in at least one of the two group comparisons, we assessed genes with altered TE using DAVID GO term clustering. This analysis revealed that upon *mrps-5* RNAi, genes with a high TE were coding for membrane components, proteins involved in stabilization of membrane potential, and proteins used in oxygen transport that include genes such as *aat-7*, *dpy-19*, and *rom-5* (Figures 2E and 2F; Table S2). This observation is likely reflecting the worm's need to adapt to its altered mitochondrial biology. Strikingly, genes with a low TE were by and large coding for proteins involved in translation and ribosome biogenesis (Figure 2E; Table S2), suggesting that *mrps-5* RNAi worms suppress the translation of cytosolic ribosome components. These genes included translation elongation factors such as *eif-3.B*, *eif-3.C*, and *eif-3.D* (Figure 2F), in addition to those coding for the vast majority of RPs. Remarkably, visualizing the TE of the ribosome-associated proteins individually highlights what amounts to be almost a complete repression of the genes coding for the RPs that assemble the cytosolic ribosome (Figure 2G). These findings demonstrate the *mrps-5*-deficient mitochondrial translation machinery wields a strong regulatory influence over the cytosolic ribosomal translation machinery.

mrps-5 Worms Suppress Growth Pathways and Upregulate Stress Responses at Both the Proteome and Transcriptome Levels

To better understand how the transcriptional responses ensuing from *mrps-5* RNAi impact the proteome, we next performed both whole worm RNA-seq and sequential window acquisition of all theoretical (SWATH) mass spectrometry proteomics of *mrps-5* RNAi versus empty vector control worms. Our whole-worm RNA profiling tracked the abundances of over 16,000 transcripts (Table S3), whereas proteomics was able to quantify over 1,700 proteins (Table S4). Again, the worm samples were readily distinguished through PLS-DA (Figures 3A–3C), attributable to the large differences inherent between *mrps-5* RNAi worms and controls reflected at both the transcript and protein levels. Using the VIP scores from the PLS-DA classification, we found major changes in the *mrps-5* RNAi worms. These are characterized by an upregulation of oxidation-reduction and glycolysis-related genes and a downregulation of development, growth, and reproduction-related genes at the transcript level (Table S3). At the protein level, we found an upregulation of mitochondrial (transit peptides) and nucleosome assembly proteins and a downregulation of the mitochondrial respiratory chain (complex I) subunits along with proteins involved in development and reproduction (Table S4).

To better understand whether the changes detected at the transcript and protein levels were representative of one another, we assessed the 1,407 protein-transcript pairs overlapping between both "omics" datasets (Table S5). Given their good correlation in abundance (Figures 3D and 3E), we proceeded to check

(E) Top 10 biological processes with highest enrichments scores in low TE (blue) or high TE (yellow) transcripts using DAVID analysis clusters enrichments in Gene Ontologies (GO). Decreased TE was observed in pathways such as ribosome biogenesis and translation. Clusters with an "enrichment score" above 1.3 ($p < 0.05$, indicated with dotted line) were considered significantly enriched.

(F) Selection of mRNAs with either low TE (blue) or high TE (yellow), which contributed to the biological enrichments ("translation" or "integral component of membrane," respectively). Boxplots depict abundances (counts per million) of mRNA in the monosome and polysome for control and *mrps-5* RNAi treated worms, used to calculate TEs.

(G) Individual cytosolic ribosomal proteins have a low TE in *mrps-5* RNAi compared to control worms.

See also Figure S2 and Table S2.

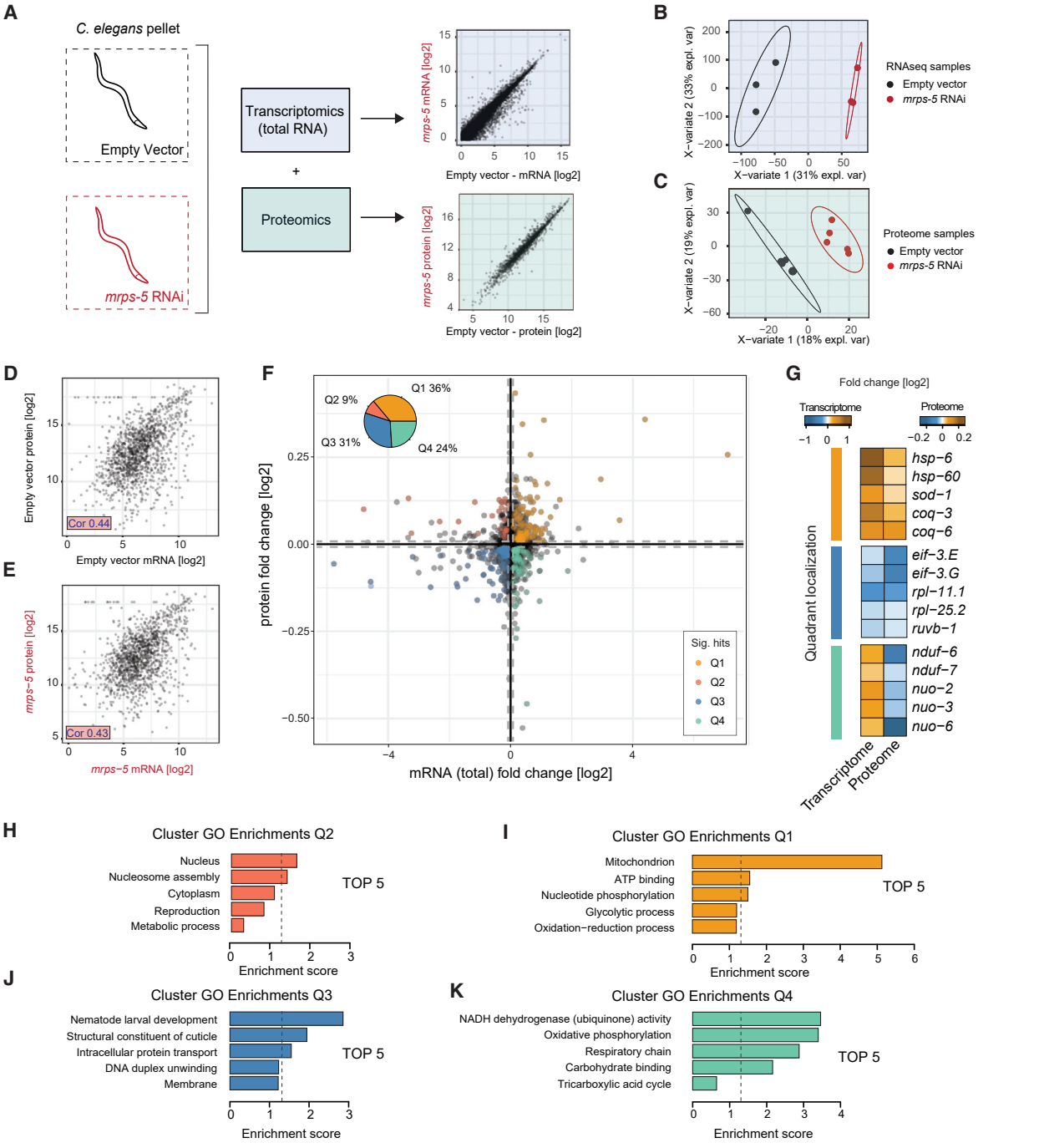

Figure 3. Proteome-Transcriptome Cross-Comparison of *mrps-5* RNAi Worms Reveals Transcriptional Suppression of Growth Pathways and Upregulation of Stress Responses

(A) Schematic showing RNA (light blue) and proteins (light green) isolated from whole worms for RNA-seq or SWATH proteomics. Transcripts or proteins (Log2-transformed normalized counts) are depicted (scatterplots). RNA-seq was performed in biological triplicates and proteomics was performed in biological quintuple per condition.

(B and C) PLS-DA for transcriptome (B) and proteome (C) shows clear distinction between *mrps-5* RNAi and control samples. PLS-DA was used to derive VIP scores for genes contributing most to the group separation.

(D and E) Significant correlations of 0.44 and 0.43 were observed in the fold changes between the 1,407 transcript-protein pairs overlapping the mRNA-protein datasets for control (D) and *mrps-5* RNAi (E) samples, respectively.

(F) Co-regulation plot of transcript and protein fold changes of *mrps-5* RNAi versus control samples. Quadrants are defined as Q1 co-upregulated, Q2 post-transcriptionally increased, Q3 co-downregulated, and Q4 post-transcriptionally suppressed. Dashed lines indicate cutoff used to eliminate noise of near 0-fold

(legend continued on next page)

their differences in a co-regulation analysis. This was achieved by investigating fold changes occurring at the transcript level versus those occurring at the protein level for each individual gene and protein (Figure 3F). To reduce noise, we omitted genes with near 0-fold changes (those within dashed lines in Figure 3F) and again used the PLS-DA-derived (Figures 3B and 3C) VIP scores for selection criteria, whereby a VIP score >1 identified genes contributing to the difference between control and *mrps-5* RNAi-treated worms. Our co-regulation analysis showed that the majority (67%) of genes were similarly regulated at the protein and transcript levels in *mrps-5* RNAi worms (Figure 3F, pie chart inset and scatterplot, in which 36% were co-upregulated [Q1] and 31% were co-downregulated [Q3]). Manual inspection of co-upregulated (Q1) genes revealed an increase in antioxidant-related defense genes such as *sod-1*, *coq-3*, and *coq-6* as well as the UPR^{mt} proteins *hsp-6* and *hsp-60*, the latter of which are in line with what we previously reported (Houtkooper et al., 2013). Co-downregulated genes (Q3) included growth- and translation-related genes such as *eif-3.E*, *eif-3.G*, *rpl-11.1*, and *rpl-25.2* (Figure 3G). Whereas only a minority (9%) of genes were downregulated at the transcript level and upregulated at the protein level (Q2), our co-regulation analysis demonstrated that a sizeable proportion of genes (24%) exhibited an upregulation at the transcript level and a downregulation at the protein level (Q4). Manual inspection showed these genes to be predominantly related to cellular respiration, such as the NADH:ubiquinone oxidoreductase core subunit genes *nduf-6*, *nduf-7*, *nuo-2*, *nuo-3*, and *nuo-6* (Figure 3G). Whereas the upregulation at the mRNA level likely reflects the worm's need to adapt to a loss of respiratory capacity from *mrps-5* RNAi, the OXPHOS complexes cannot be assembled properly because of the lack of their mitochondrial-translated partners and are downregulated on the protein level.

To better understand changes present in each quadrant of our co-regulation plot, we performed GO term enrichment analyses (Figures 3H–3K; Table S5). Whereas the genes associated with upregulated proteins and downregulated transcripts had relatively few enriched GO terms (Figure 3H), the remaining quadrants showed strong enrichments. Co-upregulated (Q1) genes enriched for mitochondrial-related processes likely reflect an active adaptation in mitochondria to the knockdown of *mrps-5* (Figure 3I). Co-downregulated (Q3) gene enrichments supported a role for decreased growth and development, with such terms as "nematode larval development" and "structural constituent of cuticle" being most prominent (Figure 3J). Meanwhile, as observed in the individual gene analysis, genes with upregulated transcripts and downregulated proteins showed enrichments for OXPHOS (Figure 3K). Taken together, co-suppression of the individual translation-related genes in Q2 (Figure 3G) with the suppression of developmental-related processes (Figure 3J) supports the idea that mitochondrial ribosomes crosstalk with cytosolic growth pathways to adapt the worm to a low energy state. Indeed, this adaptation is reflected in protein components of the worm's respiratory chain, in which OXPHOS proteins were suppressed despite their transcriptional upregulation (Figures 3G and 3K).

The Mitochondrial-to-Cytosolic Translation Response and Lifespan Are Dependent on the *atf-5/Atf4* Transcription Factor but Can Be Decoupled from Metabolic Phenotypes

Our proteome-transcriptome co-regulation analysis of *mrps-5* RNAi worms indicates that the increase of cytoprotective genes and decrease of growth and biogenesis-related genes is to a significant extent a transcriptionally regulated phenotype. This suggests that transcription factors may be core mediators of this process. Recent studies identified the transcription factor *Atf4* (*atf-5* in *C. elegans*) as a key player in communication from mitochondria toward the cytosol during mitochondrial stress induced by inhibition of either mitochondrial import, OXPHOS, membrane potential, or mitochondrial translation (Quirós et al., 2017). Elevated levels of ATF4 were also observed in many mouse longevity models that involve the suppression of cytosolic translation (Li et al., 2014). Given these reports, we investigated a potential role of *C. elegans atf-5* in coordinating the balance between cytosolic and mitochondrial translation. Using polysome profiling, we observed that the decreased cytosolic translation occurring in *mrps-5* RNAi worms is almost fully restored to control levels upon additional feeding of *atf-5* RNAi to worms (Figures 4A, S3A, and S3B). Indeed, quantification of the peaks in the polysome profiles showed significant rescue of the repressed polysomal peaks in *mrps-5* worms when *atf-5* was also knocked down (Figures 4B, S3A, and S3B). This epistasis experiment implicated *atf-5* as a mediator of the suppression of cytosolic translation that is induced by the suppression of mitochondrial translation via *mrps-5* knockdown.

In order to test if *atf-5* also plays a role in the lifespan extension of *mrps-5* RNAi worms, we performed lifespan experiments in which we silenced both *mrps-5* and *atf-5* through double RNAi (Figure 4C). We observed significant lifespan extension in the *mrps-5* RNAi treated worms as reported before (Houtkooper et al., 2013). This lifespan extension was dependent on *atf-5* because the *mrps-5/atf-5* double RNAi condition led to a marked reduction of lifespan compared to *mrps-5* RNAi alone, although it was not a complete reversal of the lifespan of controls (Figure 4C; Table S6).

In addition to repressed cytosolic translation, *mrps-5* RNAi worms also have metabolic phenotypes, including reduced respiration (Houtkooper et al., 2013). We next aimed to elucidate whether the changes in translation can be decoupled from changes in metabolism. Because both the cytosolic translation and lifespan phenotype were dependent on *atf-5*, we explored if *atf-5* RNAi also rescued the metabolic phenotypes. As described before, we found lower basal respiration in *mrps-5* RNAi-treated

change (mRNA and protein cutoffs each relative to the standard deviation of their distributions), and VIP scores >1 for both mRNA and protein levels were considered as significant hits. Pie chart inset shows percentage regulated, revealing a majority of changes being co-regulated.

(G) Examples of co-upregulated, co-downregulated, or post-transcriptionally suppressed genes, derived from the significant hits of (F).

(H–K) Top five biological processes enriched in each quadrant of the co-regulation plot, derived from the significant hits of (F). (H) pertains to Q2, (I) Q1, (J) Q3, and (K) Q4.

See also Tables S3, S4, and S5.

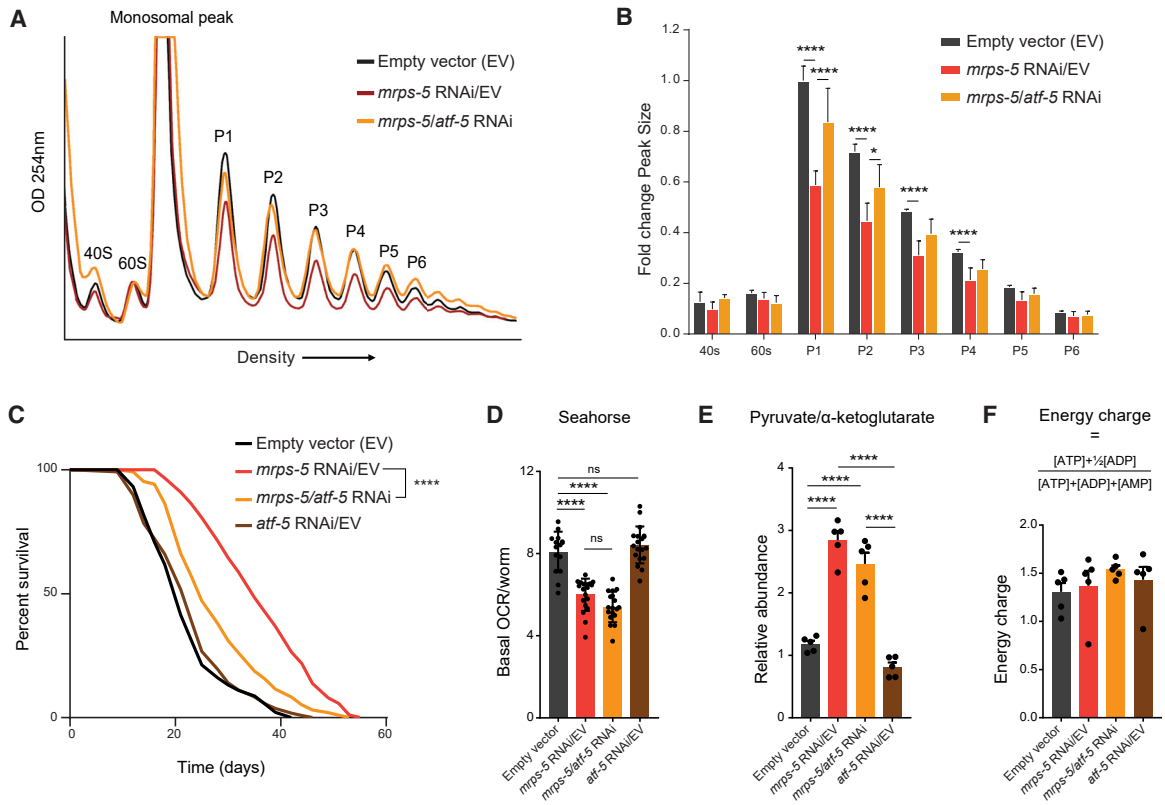

Figure 4. *Atf-5* Mediates the Balance between Mitochondrial and Ribosomal Protein Translation and Lifespan Extension, but Not the Metabolic Phenotype in *mrps-5* RNAi Worms

(A) Representative polysome profiles of control (black), *mrps-5* RNAi/EV (red), and *mrps-5* RNAi + *atf-5* RNAi (yellow) worms show *mrps-5* mediated cytosolic translational suppression is dependent on the *atf-5* transcription factor. Lysate is normalized to protein levels. The subunits (40S and 60S), monosomal peak (80S), and polysomal peak numbers are indicated (P1–P6).

(B) Quantification of polysome peak sizes of representative experiment with n = 4 per condition normalized to P1 peak of empty vector control worms. Bars represent mean ± SD and significance was tested with Student's t test, and p values were adjusted to correct for multiple testing using the Holm-Šídák method, with $\alpha = 0.05$.

(C) Lifespan curves of control (black), *mrps-5* RNAi (red), and *mrps-5/atf-5* RNAi (yellow) and *atf-5* RNAi (brown) worms show *mrps-5*-mediated lifespan extension is dependent on the *atf-5* transcription factor. n = 120 worms per condition. Survivival curves were compared using the Log-rank (Mantel-Cox) method.

(D) Seahorse respirometry measurements of control, *mrps-5* RNAi/EV, *mrps-5/atf-5* double RNAi, and *atf-5* RNAi/EV worms show reduced basal oxygen consumption rate (OCR) in both *mrps-5* RNAi/EV and *mrps-5/atf-5* RNAi-treated worms compared to controls. Data points represent average OCR per worm per well, with 15–19 wells per condition. Bars represent mean ± SEM, significance was tested with Student's t test, and p values were adjusted to correct for multiple testing using the Holm-Šídák method, with $\alpha = 0.05$.

(E) Ratio between the relative abundances of pyruvate (glycolysis) and α-ketoglutarate (TCA cycle) of control, *mrps-5* RNAi/EV, *mrps-5/atf-5* double RNAi, and *atf-5* RNAi/EV worms shows a similar metabolic shift toward glycolysis in both *mrps-5* RNAi/EV and *mrps-5/atf-5* RNAi-treated worms compared to control worms as measured by mass spectrometry. Bars represent mean ± SEM with n = 5 per condition, significance was tested with Student's t test, and p values were adjusted to correct for multiple testing using the Holm-Šídák method, with $\alpha = 0.05$.

(F) No difference was observed in energy charge measured by mass spectrometry. Bars represent mean ± SEM with n = 5 per condition and significance was tested with Student's t test, and p values were adjusted to correct for multiple testing using the Holm-Šídák method, with $\alpha = 0.05$.

See also Figure S3 and Table S6.

worms compared to the control worms (Houtkooper et al., 2013) (Figure 4D). When these worms were simultaneously treated with *atf-5* RNAi (to block the cross-organellar translational feedback), basal respiration remained similar to that of the *mrps-5* RNAi-treated worms. This indicates that *atf-5* RNAi does not rescue the reduced mitochondrial respiration in the *mrps-5* RNAi worms. To substantiate these observations, we performed metabolomics on the worms subjected to these various RNAi conditions. In line with the reduced mitochondrial activity, we observed lower amounts of tricarboxylic acid (TCA) cycle intermediates in the *mrps-5* worms compared to control worms (Figure S3C). This was accompanied by increased pyruvate levels (Figure S3C), suggesting increased glycolysis as a probable means to maintain energy homeostasis in the *mrps-5* RNAi-treated worms. Taking the ratio between a TCA cycle intermediate (α-ketoglutarate) and a glycolysis intermediate (pyruvate), we see a significant shift from mitochondrial metabolism toward glycolysis in the *mrps-5* worms (Figure 4E). Again, when these worms were simultaneously treated with both *mrps-5* and *atf-5* RNAi, a similar metabolic shift was observed, just like in *mrps-5* RNAi alone (Figure 4E). Finally, from our metabolomics data we calculated the energy charge, an index used to measure the energy

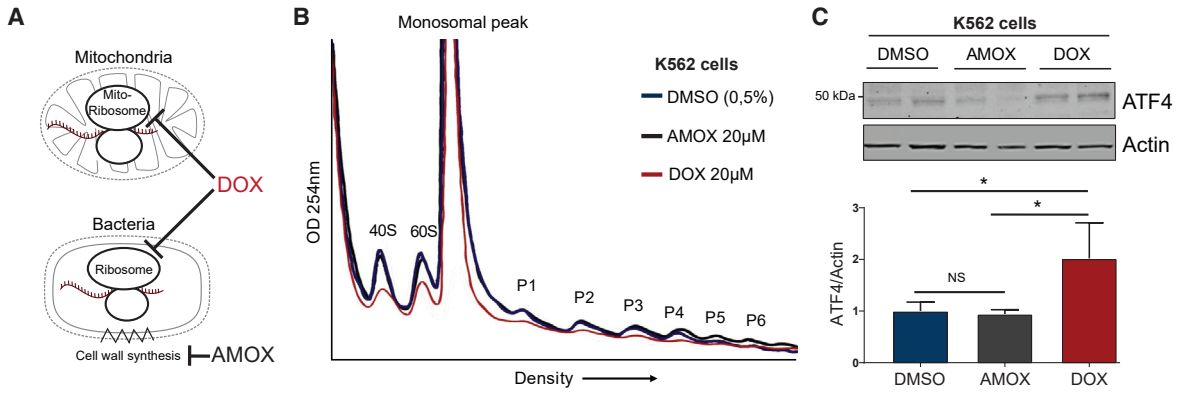

Figure 5. The Balance between Mitochondrial and Ribosomal Protein Translation Is Conserved in Human Cells

(A) Schematic of doxycycline (DOX)-mediated inhibition of mitochondrial ribosomes with amoxicillin (AMOX) not interfering with mitochondria as control antibiotic.

(B) Polysome profiles of DMSO and AMOX controls and DOX-treated K562 cells show doxycycline-induced suppression of cytosolic translation.

(C) Western blot analyses of AMOX control and DOX-treated K562 cells show DOX-induced expression of ATF4. Bars represent mean ± SD and significance was tested with one-way ANOVA with multiple comparisons, with $\alpha = 0.05$.

status: ([ATP]+½[ADP])/([ATP]+[ADP]+[AMP]). We observed no changes between worms subjected to any of the different RNAi conditions (Figure 4F). These data again support the notion that metabolic changes imposed by *mrps-5* RNAi are not causing the changes in cytosolic translation.

Moreover, we found that the mito-cytosolic translational balance does not depend on the UPR^{mt}. In the *atfs-1(cmh15)* mutant, which is unable to mount a UPR^{mt} response (Deng et al., 2019), we found that the expression of cytosolic translation genes *eif-3.c*, *eif3-g*, and *rpl-14* was still downregulated upon *mrps-5* RNAi (Figure S3D). Furthermore, although it was recently suggested that ATF4/ATF-5 displays crosstalk with the oxidative stress-response transcription factor NRF2/SKN-1 (Kasai et al., 2019), reactive oxygen species (ROS) was not induced following either *mrps-5* RNAi or doxycycline treatment, and supplementation with the antioxidant N-acetylcysteine did not suppress the lifespan extension in these conditions, suggesting independence from oxidative stress signaling (Houtkooper et al., 2013). In line with this, double knockdown of both *mrps-5* and *skn-1* still repressed the expression of *eif-3.c*, *eif-3.g*, and *rpl-14*, similar to *mrps-5* RNAi alone, suggesting that this repression is independent of *skn-1* (Figure S3E).

In conclusion, we show that *atf-5* is specifically regulating the mito-cytosolic translational balance and lifespan extension in *mrps-5* worms, whereas our respiration and metabolomics measurements allow us to decouple mitochondrial respiration from cytosolic translation in our model with altered mitochondrial translation.

The Mitochondrial-to-Cytosolic Translation Response Is Conserved in Mammalian Cells

In order to see if this communication between mitochondrial translation machinery and cytosolic translation machinery is conserved in mammalian cells, we turned to a pharmacological model of reducing mitochondrial translation with the antibiotic doxycycline. Doxycycline is in the tetracycline family of antibiotics that inhibits mitochondrial translation by binding the 30S mitochondrial ribosomal subunit, whereas other antibiotics such as amoxicillin target bacterial cell wall synthesis. Amoxicillin is used here as a control in line with our previous work (Houtkooper et al., 2013; Moullan et al., 2015) (Figure 5A). The human K562 leukemia cell line was treated with DMSO, amoxicillin, or doxycycline and subjected to polysome profiling. We found that doxycycline treatment resulted in an overall repression of all peaks, including the monosomal and polysomal fractions, revealing a global repression of cytosolic translation as a result of mitochondrial translation inhibition (Figure 5B). In line with our observations that the *C. elegans atf-5* is involved in this response, we observed that protein expression of ATF4, the mammalian homolog of *atf-5*, is upregulated in doxycycline- but not amoxicillin-treated K562 cells (Figure 5C). Taken together, these findings suggest that ATF4/*atf-5* is mediating the communication between mitochondrial and cytosolic translation machineries in a manner that is conserved from nematodes to mammals.

The Mitochondrial-to-Cytosolic Translation Response Is Conserved *In Vivo* in Mice

Having observed a conserved repression of cytosolic translation upon inhibition of mitochondrial translation in mammalian cells with doxycycline treatment, we next investigated these effects *in vivo* in mice. We treated mice for 2 weeks with doxycycline or amoxicillin in their drinking water, using doses that were previously reported to induce a mitonuclear protein imbalance (Moullan et al., 2015). To eliminate potential indirect effects of the antibiotics through the microbiome, we performed the antibiotic treatments on germ-free C57BL/6J mice. We found that doxycycline treatment resulted in suppression of global translation in liver in a dose-dependent manner (Figures S4A and S4B). Following this, we performed RNA-seq of the polysomal and total RNAs of liver tissue harvested from the antibiotic-treated mice (Figure 6A; Table S7). Similar to what was observed in worms, we found the samples were readily classified through PLS-DA (Figures 6B and 6C) and again used VIP scores to distinguish differentially expressed genes (VIP > 1). DAVID analysis of the RNA-seq results showed a striking downregulation of translation-related mRNAs in the polysomal RNA fractions of

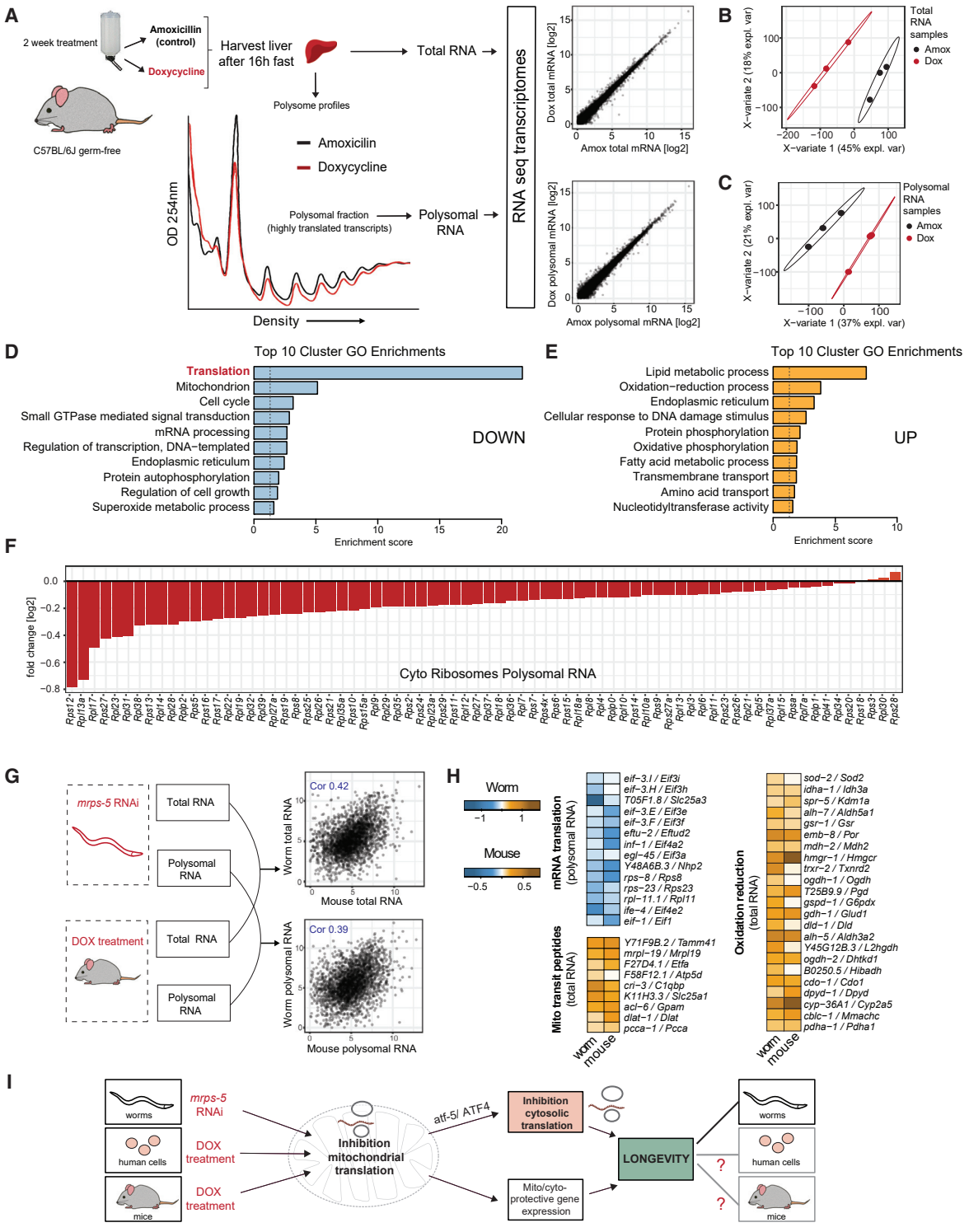

Figure 6. Suppressing Mitochondrial Ribosomes by Doxycycline Treatment Suppresses Cytosolic Ribosome Abundance *In Vivo* in Mice Liver, Resulting in a Conserved Transcriptional Signature for Longevity Assurance

(A) Schematic showing RNA isolated from either the polysomal fraction or total RNA from livers of germ-free mice treated with either DOX (red) or AMOX control (black). Transcripts (Log2 transformed normalized counts) are depicted (scatterplots). For RNA-seq, biological triplicates were used for each condition.

(B and C) PLS-DA for total (B) and polysomal (C) RNA libraries showing clear distinction between AMOX- and DOX-treated samples. Analysis was used to derive VIP scores for genes contributing most to the group separation.

(legend continued on next page)

doxycycline-treated mice (Figure 6D; Table S7) and an upregulation of various cellular defense processes including oxidation reduction (Figure 6E), which is in line with our observations in *mrps-5* deficient *C. elegans*. This suppression of cytosolic ribosomes was greater in the polysomal RNA fraction (Figure 6F) than in total RNA (Figure S4C), resulting in a suppression of the TE of ribosomal genes occurring in doxycycline-treated mice (Figure S4D; Table S7). Mitochondrial ribosomes were most strongly suppressed at the total RNA level (Figures S4E and S4F). In line with our findings in *C. elegans*, DAVID enrichment analyses showed cytoprotective processes to have high TEs and developmental processes to have low TEs, and visual inspection confirmed the near total suppression of RP genes' TEs (Figure S4D; Table S7). Taken together, these findings indicate that *in vivo* pharmacological inhibition of mitochondrial translation co-suppresses cytosolic translation, directly reducing cytosolic RP transcript TE. This confirms that the balance between mitochondrial and cytosolic translation is conserved in nematodes and mammals.

Having observed a strong conservation of the molecular phenotypes in *mrps-5* RNAi-treated worms and doxycycline-treated mouse livers, we next asked what molecular signatures were specifically conserved between the two models. To do so, we performed a mouse-worm cross-species comparison of both total and polysomal RNA-seq libraries for orthologous genes (Figure 6G). Total and polysomal RNA abundances showed interspecies correlations of 0.42 and 0.39, respectively. Assessing the overlap of differentially expressed murine and *C. elegans* genes (Figure 6H) showed a conserved upregulation of genes coding for mitochondrial transit peptides and oxidation reduction in the total RNA and a downregulation of genes involved in mRNA translation in the polysomal RNA (Table S8).

Taken all together, our findings suggest that a conserved program for mito-cytosolic translational balance is activated across species when mitochondrial translation is inhibited by distinct and diverse methods. Our findings demonstrate that this leads to ATF4/*atf-5*-mediated signaling to slow down cytosolic translation while upregulating cyto-protective genes. Considering the remarkable longevity induced by *mrps-5* and doxycycline treatments (Houtkooper et al., 2013), we propose that mito-cytosolic translational balance can ultimately be used to assure longevity in *C. elegans* and possibly also other organisms (Figure 6I).

DISCUSSION

In this study, we used a systems biology approach operating on multiple levels of biology to elucidate the relationship between mitochondrial and cytosolic translation. This included analyzing mouse population transcriptomics, worm proteome-transcriptome regulation, and polysome fractioned transcriptomics from both worms and mice with impaired mitochondrial ribosomes. Through this approach, we identified a mito-cytosolic translational balance whereby the functional ability and abundance levels of mitochondrial ribosomes are communicated to the cytosolic ribosomes to suppress cytosolic translation. This was found conserved across species and in different genetic backgrounds. Furthermore, we have shown evidence that this communication is dependent on the transcription factor ATF4. Taken together, our findings establish the presence of a retrograde communication process between mitochondrial and cytosolic ribosomes.

Communication occurring from the cytosolic ribosomes regulates mitochondrial protein abundance (Couvillion et al., 2016; Fujiki and Verner, 1993; Surguchov et al., 1983). Indeed, mitochondria are dependent on cytosolic translation, because the vast majority of the ~1,200 mitochondrial proteins, including mitochondrial RPs, are synthesized by cytosolic ribosomes (Attimonelli et al., 2002). However, given the energy requirement for cytosolic ribosome biogenesis and function coupled with the mitochondrial function as the main source of cellular energy, a clear need exists for the cytosolic and mitochondrial ribosomes to communicate their operational state to each other. Indeed, evidence for other mechanisms of communication from the mitochondria to the nucleus has been well documented. When a mitonuclear protein imbalance occurs because of inhibition of mitochondrial translation, the UPR^{mt} is activated, which triggers a nuclear transcriptional response to ultimately restore mitochondrial proteostasis (Haynes and Ron, 2010; Houtkooper et al., 2013). However, the effect on cytosolic proteostasis in a situation in which mitochondrial translation was inhibited was still unclear. Also, a cytosolic proteostatic response occurs when mitochondrial proteins are not properly targeted to mitochondria and erroneously accumulate in the cytosol (Wrobel et al., 2015). Similarly, it has been shown that defective mitochondrial tRNA taurine modifications can also result in global cellular proteostasis activation mechanisms (Fakruddin et al., 2018), which again points to an intrinsic protein homeostasis network between the mitochondria and cytosol. Indeed, our work builds upon these prior observations of inter-organelle communication and establishes the ribosomes as cross-communicating complexes between subcellular organelles. Our findings provide a framework to better understand prior observations in mitochondrial biology. For example, dysfunction in mitochondrial ribosomes was shown to block cell proliferation prior to any loss of mitochondrial respiration (Richter et al., 2013). Our findings suggest that the mito-to-cytosolic translation balance could play a role in this anti-proliferation signal from the mitochondrial ribosomes by slowing down cytosolic translation.

(D and E) Downregulated (D) or upregulated (E) top 10 biological processes enriched in the polysomal RNA of DOX-treated mice compared to AMOX show a suppression of translation-related transcripts after DOX treatment. A VIP score >1 was used to identify differentially expressed genes.
(F) Individual cytosolic ribosomal proteins are D in the polysomal RNA in DOX-treated mouse livers.
(G) Scheme depicting mouse-worm cross-species comparison of total and polysomal RNA-seq libraries.
(H) A conserved transcriptional response for a polysomal downregulation of "mRNA translation"-related proteins and total RNA upregulation of "mito transit peptides" and "oxidation reduction"-related genes was found in the mouse-worm cross-species comparison (related to G).
(I) Model depicting how downregulating mitochondrial translation results in a coordinated downregulation of cytosolic translation via *Atf4*/*atf-5*, along with an upregulation of mito-protective gene pathways ultimately leading toward longevity in *C. elegans* and possibly mammals.
See also Figure S4 and Tables S7 and S8.

Similarly, our findings can help explain the anti-carcinogenic activity of antibiotics such as doxycycline and tigecycline (Kuntz et al., 2017; Skrtić et al., 2011). With cytosolic translation already established as a target for cancer therapy (Bhat et al., 2015; Faller et al., 2015; Pelletier et al., 2018), our work points to the possibility that this could be achieved through the cellular mechanisms in place to achieve mito-cytosolic translation balance.

The loss of respiration is one of the downstream effects of impaired mitochondrial translation in the *mrps-5* worms (Houtkooper et al., 2013). Although we observed a strong upregulation of transcripts coding for mitochondrial OXPHOS proteins, the levels of these proteins were in fact downregulated in a way that likely explains the observed loss of respiration. OXPHOS in the mitochondria is carried out by five different protein complexes, four of which are dependent on mtDNA-encoded subunits. Interestingly, many of the genes that were up at the transcript level and down at the protein level (such as *nuo−6*, *nuo−3*, *nuo−2*, *nduf−7*, and *nduf−6*) were mainly nuclear genes coding for OXPHOS complex I proteins. The vast majority of OXPHOS complex I proteins are transcribed from nuclear DNA (38 genes) compared to mtDNA (7 genes) (Bar-Yaacov et al., 2012), suggesting the *mrps-5* worms may be trying to redress their loss of respiration capacity by upregulating translation of complex proteins. However, the translation impairment of mtDNA-encoded components of OXPHOS complexes and the resulting stochiometric imbalance make it seem likely that the unassembled nuclear-encoded complex proteins are degraded. This, in turn, may aggravate mitochondrial proteotoxic stress. Interestingly, this protein-specific degradation of members of stoichiometric complexes was observed before in human fibroblast (Liu et al., 2017). We suggest that mitochondrial (OXPHOS) proteins are degraded when they are not properly integrated in their preferred structures, i.e., the OXPHOS complexes. This has been previously reported in patients with mutations in the complex IV protein COA6, where the authors observed not only a complete absence of COA6 but also reduced levels of other complex IV proteins such as COX1, COX2, and COX4 (Baertling et al., 2015).

Inhibiting mitochondrial translation obviously leads to numerous downstream metabolic effects. Surprisingly, we showed that while *atf-5* is required for the mito-cytosolic translational balance and lifespan extension in *mrps-5* worms, it appears dispensable for the metabolic phenotypes such as mitochondrial respiration and metabolite profiles. Metabolic reprogramming is an important consequence of inhibiting mitochondrial translation, but our results suggest that this is not the driving force behind the mito-cytosolic translational balance. Rather, we propose it goes hand in hand with the mito-cytosolic translational balance regulated by *atf-5* in order to activate cytoprotection and maintain cellular homeostasis. This concept is supported by previous work showing that *mrps-5* RNAi still extends lifespan in the AMPK (*aak-2*) mutant, demonstrating that it is not exclusively metabolic effects that are important for the observed lifespan extension (Houtkooper et al., 2013).

We found that *Atf4* plays a role in orchestrating the communication from the mitoribosome to the cytoribosome. Interestingly, upregulation of this transcription factor has been linked to longevity in mice (Li et al., 2014), and overexpression of the orthologous transcription factor in yeast (GCN4) extended lifespan (Mittal et al., 2017), both in line with the longevity of *mrps-5* RNAi-treated worms (Houtkooper et al., 2013), which was dependent on *atf-5*. In the yeast overexpression study, it was observed that *Gcn4* acts as a repressor of protein synthesis (Mittal et al., 2017), in line with our observations in nematode and mammalian models. We did not observe changes in *atf-5* mRNA in our *mrps-5* RNAi-treated worm transcriptomics or in *Atf4* mRNA in our doxycycline-treated mice transcriptomics. Although the regulation of *Atf4* and its orthologs *Gcn4* and *atf-5* is not fully understood, it is known that differential contribution of two upstream open reading frames (uORFs) in the 5′ leader of the mouse *Atf4* mRNA regulates *Atf4* expression (Vattem and Wek, 2004). Translation of ATF4 can be increased by phospho-eIF2α, phosphorylated by one of the four eIF2α kinases (PERK, GCN2, PKR, HRI) (Harding et al., 2000). However, the activated ATF4 induced by mitochondrial stress (e.g., doxycycline treatment), was not dependent on any of the individual eIF2α kinases in mammalian cells (Quirós et al., 2017). More recently, it was shown that there are also GCN2- and EIF2α-independent ways to activate ATF4, for instance, in the case of methionine restriction (Mazor and Stipanuk, 2016). Understanding how ATF4 activation is regulated after inhibition of mitochondrial ribosomes may be valuable to target the aging process.

Slowing down cytosolic mRNA translation itself can extend lifespan (Hansen et al., 2007; Pan et al., 2007). Other longevity mechanisms are also known to be marked by reduced cytosolic translation such as the reduction of mTORC1 (Genolet et al., 2008) or insulin signaling (Stout et al., 2013), which both also extend lifespan in many organisms (Blüher et al., 2003; Harrison et al., 2009; Jia et al., 2004; Kaeberlein et al., 2005; Kapahi et al., 2004; Tissenbaum and Ruvkun, 1998; Vellai et al., 2003). In all likelihood, the mechanism leading to the observed reduction of cytosolic translation in the context of longevity is multifactorial. Because *C. elegans* mRNAs are known to, by and large, be lacking TOP 5′UTR sequences (Thoreen et al., 2012), it seems unlikely that the 5′UTRs are playing an important role in the regulation of mRNA translation. Therefore, we suggest an alternative mechanism may be at play involving mRNA binding proteins, many of which we found downregulated in the proteome of *mrps-5* RNAi worms. One of these downregulated proteins is polyA binding protein 2 (*pab-2*), which is associated with several ribosomal proteins and localizes to polysomes; its knockdown also results in a reduction of polysomes (Lemieux and Bachand, 2009). Exploring this and other putative mechanisms that are responsible for the repression of mRNA translation in our models of longevity will be a very exciting area of future work.

Our cross-species analyses resulted in a transcriptional signature that was changing similarly in both worms and mice upon inhibition of mitochondrial translation. Most of the upregulated hits in our signature were mitochondrial proteins suggesting a mitochondrial quality control system. This signature involved cytoprotective transcriptional changes, including an upregulation of oxidation-reduction processes, and was characterized by a reduction of translation EFs. These findings are in line with the observation that inhibiting mitochondrial translation is a conserved longevity mechanism (Houtkooper et al., 2013). Our work here shows that this inhibition can also induce a previously unknown mito-cytosolic translational balance whereby cytosolic translation is also lowered, linking to another longevity mechanism (MacInnes, 2016). Finally, we identified a cyto-protective transcriptional signature characteristic of this response, and

together these changes have the potential to drive healthy aging (Figure 5I).

Limitations of Study

Although inhibiting mitochondrial ribosomes in *C. elegans* extends lifespan and its dependence on *atf-5* was robustly demonstrated in our study, it remains to be determined whether inhibition of mitochondrial translation and activation of ATF4 can extend lifespan in mice and humans. Furthermore, because of the fact that our pharmacological intervention was an antibiotic, our work *in vivo* was carried out in germ-free mice and therefore may not fully recapitulate what may occur in wild-type mice. Likewise, our *in vivo* study focused on liver tissue, and it remains to be seen if these observations are also conserved in other tissues.

STAR★METHODS

Detailed methods are provided in the online version of this paper and include the following:

- KEY RESOURCES TABLE
- LEAD CONTACT AND MATERIALS AVAILABILITY
- EXPERIMENTAL MODEL AND SUBJECT DETAILS
  - Nematode Growing Conditions and RNAi Experiments
  - K562 Cell Culture
- METHOD DETAILS
  - BXD Strains
  - Network Analysis
  - Polysome Profiling
  - Western Blotting
  - Isolation of mRNA (Total, Monosomal, and Polysomal)
  - Library Preparation
  - Read Mapping, Statistical Analyses, and Data Visualization
  - Protein-Transcript Cross Comparison
  - SWATH Proteomics – Library Acquisition
- QUANTIFICATION AND STATISTICAL ANALYSIS
- DATA AND CODE AVAILABILITY

SUPPLEMENTAL INFORMATION

Supplemental Information can be found online at https://doi.org/10.1016/j.cmet.2020.01.011.

ACKNOWLEDGMENTS

Work in the Houtkooper group is financially supported by an ERC Starting grant (no. 638290), a VIDI grant from ZonMw (no. 91715305), and a grant from the Velux Stiftung (no. 1063). A.W.M. is supported by E-Rare-2, the ERA-Net for Research on Rare Diseases (ZonMW #40-44000-98-1008). G.E.J. is supported by a Federation of European Biochemical Society (FEBS, https://www.febs.org) long-term fellowship and a VENI grant from ZonMw (no. 09150161810014, https://www.zonmw.nl) E.G.W. was supported by an NIH F32 Ruth Kirchstein Fellowship (F32GM119190). R.A. was supported by the ERC advanced grant ERC-20140AdG 670821. M.A.M. is supported by NIH P20GM121176 and a Glenn Foundation for Medical Research and American Federation for Aging Research Junior Faculty Grant.

AUTHOR CONTRIBUTIONS

M.M., G.E.J., A.W.M., and R.H.H. conceived and designed the project. M.M., S.R., F.J., M.L., Y.J.L., and J.L. performed experiments, and G.E.J., E.G.W., A.J., P.D.M., and A.H.C.v.K. performed bioinformatics. M.M., B.V.S., and M.v.W. performed metabolomics. M.M., G.E.J., E.G.W., R.A., M.A.M., B.K.K., A.W.M., and R.H.H. interpreted data. M.M., G.E.J., A.W.M., and R.H.H. wrote the manuscript with contributions from all other authors.

DECLARATION OF INTERESTS

R.H.H. is an inventor on a patent related to mitochondrial ribosomal proteins as aging regulators. The other authors declare that they have no conflicts of interest.

Received: December 18, 2018
Revised: August 22, 2019
Accepted: January 22, 2020
Published: February 20, 2020

REFERENCES

Anders, S., Pyl, P.T., and Huber, W. (2015). HTSeq–a Python framework to work with high-throughput sequencing data. Bioinformatics *31*, 166–169.

Andrews, S. (2010). FastQC: a quality control tool for high throughput sequence data. http://www.bioinformatics.babraham.ac.uk/projects/fastqc.

Attimonelli, M., Catalano, D., Gissi, C., Grillo, G., Licciulli, F., Liuni, S., Santamaria, M., Pesole, G., and Saccone, C. (2002). MitoNuc: a database of nuclear genes coding for mitochondrial proteins. Update 2002. Nucleic Acids Res. *30*, 172–173.

Baertling, F., A M van den Brand, M., Hertecant, J.L., Al-Shamsi, A., P van den Heuvel, L., Distelmaier, F., Mayatepek, E., Smeitink, J.A., Nijtmans, L.G., and Rodenburg, R.J. (2015). Mutations in COA6 cause cytochrome c oxidase deficiency and neonatal hypertrophic cardiomyopathy. Hum. Mutat. *36*, 34–38.

Bar-Yaacov, D., Blumberg, A., and Mishmar, D. (2012). Mitochondrial-nuclear co-evolution and its effects on OXPHOS activity and regulation. Biochim. Biophys. Acta *1819*, 1107–1111.

Bhat, M., Robichaud, N., Hulea, L., Sonenberg, N., Pelletier, J., and Topisirovic, I. (2015). Targeting the translation machinery in cancer. Nat. Rev. Drug Discov. *14*, 261–278.

Blüher, M., Kahn, B.B., and Kahn, C.R. (2003). Extended longevity in mice lacking the insulin receptor in adipose tissue. Science *299*, 572–574.

Bolger, A.M., Lohse, M., and Usadel, B. (2014). Trimmomatic: a flexible trimmer for Illumina sequence data. Bioinformatics *30*, 2114–2120.

Boulesteix, A.L., and Strimmer, K. (2007). Partial least squares: a versatile tool for the analysis of high-dimensional genomic data. Brief. Bioinform. *8*, 32–44.

Buttgereit, F., and Brand, M.D. (1995). A hierarchy of ATP-consuming processes in mammalian cells. Biochem. J. *312*, 163–167.

Chiocchetti, A., Zhou, J., Zhu, H., Karl, T., Haubenreisser, O., Rinnerthaler, M., Heeren, G., Oender, K., Bauer, J., Hintner, H., et al. (2007). Ribosomal proteins Rpl10 and Rps6 are potent regulators of yeast replicative life span. Exp. Gerontol. *42*, 275–286.

Couvillion, M.T., Soto, I.C., Shipkovenska, G., and Churchman, L.S. (2016). Synchronized mitochondrial and cytosolic translation programs. Nature *533*, 499–503.

Deng, P., Uma Naresh, N., Du, Y., Lamech, L.T., Yu, J., Zhu, L.J., Pukkila-Worley, R., and Haynes, C.M. (2019). Mitochondrial UPR repression during *Pseudomonas aeruginosa* infection requires the bZIP protein ZIP-3. Proc. Natl. Acad. Sci. USA *116*, 6146–6151.

Fakruddin, M., Wei, F.Y., Suzuki, T., Asano, K., Kaieda, T., Omori, A., Izumi, R., Fujimura, A., Kaitsuka, T., Miyata, K., et al. (2018). Defective Mitochondrial tRNA Taurine Modification Activates Global Proteostress and Leads to Mitochondrial Disease. Cell Rep. *22*, 482–496.

Faller, W.J., Jackson, T.J., Knight, J.R., Ridgway, R.A., Jamieson, T., Karim, S.A., Jones, C., Radulescu, S., Huels, D.J., Myant, K.B., et al. (2015). mTORC1-mediated translational elongation limits intestinal tumour initiation and growth. Nature *517*, 497–500.

Fujiki, M., and Verner, K. (1993). Coupling of cytosolic protein synthesis and mitochondrial protein import in yeast. Evidence for cotranslational import in vivo. J. Biol. Chem. *268*, 1914–1920.

Genolet, R., Araud, T., Maillard, L., Jaquier-Gubler, P., and Curran, J. (2008). An approach to analyse the specific impact of rapamycin on mRNA-ribosome association. BMC Med. Genomics *1*, 33.

Greber, B.J., Boehringer, D., Leibundgut, M., Bieri, P., Leitner, A., Schmitz, N., Aebersold, R., and Ban, N. (2014). The complete structure of the large subunit of the mammalian mitochondrial ribosome. Nature *515*, 283–286.

Greber, B.J., Bieri, P., Leibundgut, M., Leitner, A., Aebersold, R., Boehringer, D., and Ban, N. (2015). Ribosome. The complete structure of the 55S mammalian mitochondrial ribosome. Science *348*, 303–308.

Hansen, M., Taubert, S., Crawford, D., Libina, N., Lee, S.J., and Kenyon, C. (2007). Lifespan extension by conditions that inhibit translation in Caenorhabditis elegans. Aging Cell *6*, 95–110.

Harding, H.P., Novoa, I., Zhang, Y., Zeng, H., Wek, R., Schapira, M., and Ron, D. (2000). Regulated translation initiation controls stress-induced gene expression in mammalian cells. Mol. Cell *6*, 1099–1108.

Harrison, D.E., Strong, R., Sharp, Z.D., Nelson, J.F., Astle, C.M., Flurkey, K., Nadon, N.L., Wilkinson, J.E., Frenkel, K., Carter, C.S., et al. (2009). Rapamycin fed late in life extends lifespan in genetically heterogeneous mice. Nature *460*, 392–395.

Haynes, C.M., and Ron, D. (2010). The mitochondrial UPR - protecting organelle protein homeostasis. J. Cell Sci. *123*, 3849–3855.

Houtkooper, R.H., Mouchiroud, L., Ryu, D., Moullan, N., Katsyuba, E., Knott, G., Williams, R.W., and Auwerx, J. (2013). Mitonuclear protein imbalance as a conserved longevity mechanism. Nature *497*, 451–457.

Huang da, W., Sherman, B.T., and Lempicki, R.A. (2009). Systematic and integrative analysis of large gene lists using DAVID bioinformatics resources. Nat. Protoc. *4*, 44–57.

Jia, K., Chen, D., and Riddle, D.L. (2004). The TOR pathway interacts with the insulin signaling pathway to regulate C. elegans larval development, metabolism and life span. Development *131*, 3897–3906.

Jovaisaite, V., and Auwerx, J. (2015). The mitochondrial unfolded protein response—synchronizing genomes. Curr. Opin. Cell Biol. *33*, 74–81.

Kaeberlein, M., Powers, R.W., 3rd, Steffen, K.K., Westman, E.A., Hu, D., Dang, N., Kerr, E.O., Kirkland, K.T., Fields, S., and Kennedy, B.K. (2005). Regulation of yeast replicative life span by TOR and Sch9 in response to nutrients. Science *310*, 1193–1196.

Kapahi, P., Zid, B.M., Harper, T., Koslover, D., Sapin, V., and Benzer, S. (2004). Regulation of lifespan in Drosophila by modulation of genes in the TOR signaling pathway. Curr. Biol. *14*, 885–890.

Kasai, S., Yamazaki, H., Tanji, K., Engler, M.J., Matsumiya, T., and Itoh, K. (2019). Role of the ISR-ATF4 pathway and its cross talk with Nrf2 in mitochondrial quality control. J. Clin. Biochem. Nutr. *64*, 1–12.

Kim, D., Langmead, B., and Salzberg, S.L. (2015). HISAT: a fast spliced aligner with low memory requirements. Nat. Methods *12*, 357–360.

Koopman, M., Michels, H., and Dancy, B.M. (2016). A screening-based platform for the assessment of cellular respiration in Caenorhabditis elegans. Nat Protoc. *11*, 1798–1816.

Kuhn, A., Luthi-Carter, R., and Delorenzi, M. (2008). Cross-species and cross-platform gene expression studies with the Bioconductor-compliant R package 'annotationTools'. BMC Bioinformatics *9*, 26.

Kuntz, E.M., Baquero, P., Michie, A.M., Dunn, K., Tardito, S., Holyoake, T.L., Helgason, G.V., and Gottlieb, E. (2017). Targeting mitochondrial oxidative phosphorylation eradicates therapy-resistant chronic myeloid leukemia stem cells. Nat. Med. *23*, 1234–1240.

Lane, N., and Martin, W. (2010). The energetics of genome complexity. Nature *467*, 929–934.

Law, C.W., Chen, Y., Shi, W., and Smyth, G.K. (2014). voom: Precision weights unlock linear model analysis tools for RNA-seq read counts. Genome Biol. *15*, R29.

Lemieux, C., and Bachand, F. (2009). Cotranscriptional recruitment of the nuclear poly(A)-binding protein Pab2 to nascent transcripts and association with translating mRNPs. Nucleic Acids Res. *37*, 3418–3430.

Li, W., Li, X., and Miller, R.A. (2014). ATF4 activity: a common feature shared by many kinds of slow-aging mice. Aging Cell *13*, 1012–1018.

Liu, Y., Borel, C., Li, L., Muller, T., Williams, E.G., Germain, P.L., Buljan, M., Sajic, T., Boersema, P.J., Shao, W., et al. (2017). Systematic proteome and proteostasis profiling in human Trisomy 21 fibroblast cells. Nat Commun. *8*, 1212.

Liu, Y., McIntyre, R., Janssens, G., Williams, E., Lan, J., van Veen, H., van der Wel, N., Mair, W.B., Aebersold, R., MacInnes, A., et al. (2019). Mitochondrial translation and dynamics synergistically extend lifespan in C. elegans through HLH-30. bioRxiv. https://doi.org/10.1101/871079.

MacInnes, A.W. (2016). The role of the ribosome in the regulation of longevity and lifespan extension. Wiley Interdiscip. Rev. RNA *7*, 198–212.

Mazor, K.M., and Stipanuk, M.H. (2016). GCN2- and eIF2α-phosphorylation-independent, but ATF4-dependent, induction of CARE-containing genes in methionine-deficient cells. Amino Acids *48*, 2831–2842.

Mittal, N., Guimaraes, J.C., Gross, T., Schmidt, A., Vina-Vilaseca, A., Nedialkova, D.D., Aeschimann, F., Leidel, S.A., Spang, A., and Zavolan, M. (2017). The Gcn4 transcription factor reduces protein synthesis capacity and extends yeast lifespan. Nat. Commun. *8*, 457.

Molenaars, M., Janssens, G.E., Santermans, T., Lezzerini, M., Jelier, R., MacInnes, A.W., and Houtkooper, R.H. (2018). Mitochondrial ubiquinone-mediated longevity is marked by reduced cytoplasmic mRNA translation. Life Science Alliance *1*, e201800082.

Moullan, N., Mouchiroud, L., Wang, X., Ryu, D., Williams, E.G., Mottis, A., Jovaisaite, V., Frochaux, M.V., Quiros, P.M., Deplancke, B., et al. (2015). Tetracyclines Disturb Mitochondrial Function across Eukaryotic Models: A Call for Caution in Biomedical Research. Cell Rep. *10*, 1681–1691.

Narayan, V., Ly, T., Pourkarimi, E., Murillo, A.B., Gartner, A., Lamond, A.I., and Kenyon, C. (2016). Deep Proteome Analysis Identifies Age-Related Processes in C. elegans. Cell Syst. *3*, 144–159.

Neuwirth, E. (2014). RColorBrewer: ColorBrewer Palettes. R package version 1.1-2. https://cran.r-project.org/web/packages/RColorBrewer/.

Pan, K.Z., Palter, J.E., Rogers, A.N., Olsen, A., Chen, D., Lithgow, G.J., and Kapahi, P. (2007). Inhibition of mRNA translation extends lifespan in Caenorhabditis elegans. Aging Cell *6*, 111–119.

Parker, S.J., Rost, H., Rosenberger, G., Collins, B.C., Malmström, L., Amodei, D., Venkatraman, V., Raedschelders, K., Van Eyk, J.E., and Aebersold, R. (2015). Identification of a Set of Conserved Eukaryotic Internal Retention Time Standards for Data-independent Acquisition Mass Spectrometry. Mol. Cell. Proteomics *14*, 2800–2813.

Pelletier, J., Thomas, G., and Volarević, S. (2018). Ribosome biogenesis in cancer: new players and therapeutic avenues. Nat. Rev. Cancer *18*, 51–63.

Quirós, P.M., Prado, M.A., Zamboni, N., D'Amico, D., Williams, R.W., Finley, D., Gygi, S.P., and Auwerx, J. (2017). Multi-omics analysis identifies ATF4 as a key regulator of the mitochondrial stress response in mammals. J. Cell Biol. *216*, 2027–2045.

Richter, U., Lahtinen, T., Marttinen, P., Myöhänen, M., Greco, D., Cannino, G., Jacobs, H.T., Lietzén, N., Nyman, T.A., and Battersby, B.J. (2013). A mitochondrial ribosomal and RNA decay pathway blocks cell proliferation. Curr. Biol. *23*, 535–541.

Ritchie, M.E., Phipson, B., Wu, D., Hu, Y., Law, C.W., Shi, W., and Smyth, G.K. (2015). limma powers differential expression analyses for RNA-sequencing and microarray studies. Nucleic Acids Res. *43*, e47.

Robinson, M.D., McCarthy, D.J., and Smyth, G.K. (2010). edgeR: a Bioconductor package for differential expression analysis of digital gene expression data. Bioinformatics *26*, 139–140.

Rohart, F., Gautier, B., Singh, A., and Lê Cao, K.A. (2017). mixOmics: An R package for 'omics feature selection and multiple data integration. PLoS Comput. Biol. *13*, e1005752.

Röst, H.L., Rosenberger, G., Navarro, P., Gillet, L., Miladinović, S.M., Schubert, O.T., Wolski, W., Collins, B.C., Malmström, J., Malmström, L., and

Aebersold, R. (2014). OpenSWATH enables automated, targeted analysis of data-independent acquisition MS data. Nat. Biotechnol. *32*, 219–223.

Ruijter, J.M., Ramakers, C., Hoogaars, W.M., Karlen, Y., Bakker, O., van den Hoff, M.J., and Moorman, A.F. (2009). Amplification efficiency: linking baseline and bias in the analysis of quantitative PCR data. Nucleic Acids Res. *37*, e45.

Skrtić, M., Sriskanthadevan, S., Jhas, B., Gebbia, M., Wang, X., Wang, Z., Hurren, R., Jitkova, Y., Gronda, M., Maclean, N., et al. (2011). Inhibition of mitochondrial translation as a therapeutic strategy for human acute myeloid leukemia. Cancer Cell *20*, 674–688.

Smits, P., Smeitink, J.A., van den Heuvel, L.P., Huynen, M.A., and Ettema, T.J. (2007). Reconstructing the evolution of the mitochondrial ribosomal proteome. Nucleic Acids Res. *35*, 4686–4703.

Stout, G.J., Stigter, E.C., Essers, P.B., Mulder, K.W., Kolkman, A., Snijders, D.S., van den Broek, N.J., Betist, M.C., Korswagen, H.C., Macinnes, A.W., and Brenkman, A.B. (2013). Insulin/IGF-1-mediated longevity is marked by reduced protein metabolism. Mol. Syst. Biol. *9*, 679.

Surguchov, A.P., Sudarickov, A.B., Telckov, M.V., Smirnov, V.N., Ter-Avanesyan, M.D., and Inge-Vechtomov, S.G. (1983). Relationship between cytoplasmic and mitochondrial apparatus of protein synthesis in yeast Saccharomyces cerevisiae. Mol. Gen. Genet. *189*, 172–174.

Thoreen, C.C., Chantranupong, L., Keys, H.R., Wang, T., Gray, N.S., and Sabatini, D.M. (2012). A unifying model for mTORC1-mediated regulation of mRNA translation. Nature *485*, 109–113.

Tissenbaum, H.A., and Ruvkun, G. (1998). An insulin-like signaling pathway affects both longevity and reproduction in Caenorhabditis elegans. Genetics *148*, 703–717.

Vattem, K.M., and Wek, R.C. (2004). Reinitiation involving upstream ORFs regulates ATF4 mRNA translation in mammalian cells. Proc. Natl. Acad. Sci. USA *101*, 11269–11274.

Vellai, T., Takacs-Vellai, K., Zhang, Y., Kovacs, A.L., Orosz, L., and Müller, F. (2003). Genetics: influence of TOR kinase on lifespan in C. elegans. Nature *426*, 620.

Wang, X., Pandey, A.K., Mulligan, M.K., Williams, E.G., Mozhui, K., Li, Z., Jovaisaite, V., Quarles, L.D., Xiao, Z., Huang, J., et al. (2016). Joint mouse-human phenome-wide association to test gene function and disease risk. Nat. Commun. *7*, 10464.

Warnes, G.R., Bolker, B., Bonebakker, L., Gentleman, R., Huber, W., Liaw, A., Lumley, T., Maechler, M., Magnusson, A., Moeller, S., et al. (2016). gplots: Various R Programming Tools for Plotting Data. R package version 3.0.1. https://cran.r-project.org/web/packages/gplots/.

Wickham, H. (2009). ggplot2: Elegant Graphics for Data Analysis (Springer).

Wieser, W., and Krumschnabel, G. (2001). Hierarchies of ATP-consuming processes: direct compared with indirect measurements, and comparative aspects. Biochem. J. *355*, 389–395.

Williams, E.G., Wu, Y., Jha, P., Dubuis, S., Blattmann, P., Argmann, C.A., Houten, S.M., Amariuta, T., Wolski, W., Zamboni, N., et al. (2016). Systems proteomics of liver mitochondria function. Science *352*, aad0189.

Williams, E.G., Wu, Y., Wolski, W., Kim, J.Y., Lan, J., Hasan, M., Halter, C., Jha, P., Ryu, D., Auwerx, J., and Aebersold, R. (2018). Quantifying and Localizing the Mitochondrial Proteome Across Five Tissues in A Mouse Population. Mol. Cell. Proteomics *17*, 1766–1777.

Wrobel, L., Topf, U., Bragoszewski, P., Wiese, S., Sztolsztener, M.E., Oeljeklaus, S., Varabyova, A., Lirski, M., Chroscicki, P., Mroczek, S., et al. (2015). Mistargeted mitochondrial proteins activate a proteostatic response in the cytosol. Nature *524*, 485–488.

Wu, Y., Williams, E.G., and Aebersold, R. (2017). Application of SWATH Proteomics to Mouse Biology. Curr. Protoc. Mouse Biol. *7*, 130–143.

STAR★METHODS

KEY RESOURCES TABLE

REAGENT or RESOURCE	SOURCE	IDENTIFIER
Antibodies		
Rabbit monoclonal anti-ATF4 (1:1000)	Cell Signaling Technology	Cat# 11815 RRID: AB_2616025
Mouse monoclonal anti-β-Actin (1:5000)	Sigma-Aldrich	Cat# A5441 RRID: AB_476744
Donkey anti-Rabbit IgG (1:10000)	LI-COR Biosciences	Cat# 925-68073 RRID: AB_2716687
Goat anti-mouse IgG (1:10000)	LI-COR Biosciences	Cat# 925-32210 RRID: AB_2687825
Bacterial and Virus Strains		
Escherichia coli: OP50	Caenorhabditis Genetics Center	RRID:WB-STRAIN:OP50
Escherichia coli: HT115 (DE3)	Caenorhabditis Genetics Center	RRID:WB-STRAIN:HT115(DE3)
Ahringer *C. elegans* RNAi library	Source BioScience	https://www.sourcebioscience.com/products/life-science-research/clones/rnai-resources/c-elegans-rnai-collection-ahringer/
Chemicals, Peptides, and Recombinant Proteins		
Cycloheximide	Sigma-Aldrich	Cat# C6255
Doxycycline	Sigma-Aldrich	Cat# D9891
Amoxicillin	Sigma-Aldrich	Cat# A8523
DMSO	Sigma -Aldrich	Cat# D8418
5-FU	Sigma -Aldrich	Cat# f6627
Sodium azide	Sigma-Aldrich	Cat# s8032
FCCP	Abcam	Cat# ab120081
Critical Commercial Assays		
BCA protein assay Reagent A	Thermo Fisher Scientific	Cat# 23223
TRIzol (LS)	Invitrogen	Cat# 15596026 (#10296010)
RNeasy MinElute Cleanup Kit	QIAGEN	Cat# 74204
NEBNext Ultra Directional RNA Library Prep Kit	NEB	Cat# E7420
rRNA depletion kit	NEB	Cat# E6310
QuantiTect Reverse Transcription Kit	QIAGEN	Cat# 205314
LightCycler® 480 SYBR Green I Master	Roche	Cat# 04887352001
Deposited Data		
C. elegans and Mouse RNA-seq data	This paper	GEO: GSE122097
C. elegans Proteomics data	This paper	PRIDE: PXD009223
BXD mouse liver proteome data (reprocessed)	This paper	Table S1
BXD mouse liver proteome data	genenetwork.org	GN540
BXD mouse multi tissue proteome data	Molecular and Cellular Proteomics Journal	https://doi.org/10.1074/mcp.RA118.000554
Experimental Models: Cell Lines		
Human: K562 cells	ATCC	CCL-243 RRID:CVCL_0004
Experimental Models: Organisms/Strains		
C. elegans: N2 Bristol	Caenorhabditis Genetics Center (CGC); https://cbs.umn.edu/cgc/home	CGC:10570 RRID:WB-STRAIN: N2_(ancestral)
C. elegans: *atfs-1(cmh15)*	(Deng et al., 2019)	N/A
Mouse: C57BL/6J germ-free	Micalis Institute (INRA Research Center of Jouy-en-Josas)	N/A

(*Continued on next page*)

Continued

REAGENT or RESOURCE	SOURCE	IDENTIFIER
Oligonucleotides		
F35G12.2 forward primer: 5′-ACTGCGTTCATCCGTGCCGC-3′	Sigma-Aldrich	N/A
F35G12.2 reverse primer: 5′-TGCGGTCCTCGAGCTCCTTC-3′	Sigma-Aldrich	N/A
pmp-3 forward primer: 5′-GCTGGAGTCACTCATCGTGTTA −3′	Sigma-Aldrich	N/A
pmp-3 reverse primer: 5′-CCGGCCAATCATCCTCTTGA −3′	Sigma-Aldrich	N/A
mrps-5 forward primer: 5′-ACTGGCCGAACGAAAAGGTCT −3′	Sigma-Aldrich	N/A
mrps-5 reverse primer: 5′-AGTGGAAATCGGTGACGCCACAA −3′	Sigma-Aldrich	N/A
atf-5 forward primer: 5′-GTGCGAAGAAATCGAGCGTC −3′	Sigma-Aldrich	N/A
atf-5 reverse primer: 5′-GCTCCAACTCGGATACCTGAT −3′	Sigma-Aldrich	N/A
skn-1 forward primer: 5′-TCAATTTATGGAGTGTCGTCCA −3′	Sigma-Aldrich	NA
skn-1 reverse primer: 5′-CCGTTGATCATCACGCCAAC −3′	Sigma-Aldrich	N/A
eif-3.c forward primer: 5′-TTTCCAGGAAGGAACGAGCG −3′	Sigma-Aldrich	N/A
eif-3.c reverse primer: 5′-CCGTCTTGTCCTTGTCCTCC −3′	Sigma-Aldrich	N/A
eif-3.g forward primer: 5′-GCATTAACGCAATGGCTCCC −3′	Sigma-Aldrich	N/A
eif-3.g reverse primer: 5′-TCGGTACGTGTTCCATCAGC −3′	Sigma-Aldrich	N/A
rpl-14 forward primer: 5′-CAAGCTCACCGACTTCGAGA −3′	Sigma-Aldrich	N/A
rpl-14 reverse primer: 5′-GAGCTCCACTCGGACGATTC −3′	Sigma-Aldrich	N/A
Software and Algorithms		
R (v3.4.3)	R	https://www.r-project.org
FastQC	(Andrews, 2010)	https://www.bioinformatics.babraham.ac.uk/projects/fastqc/
iGraph v1.2.1 package	iGraph	https://cran.r-project.org/web/packages/igraph/
RTA v2.7.7	Illumina, Real-Time Analysis	illumina.com
Bcl2fastq v2.17	Illumina	illumina.com
Trimmomatic v0.32	(Bolger et al., 2014)	http://www.usadellab.org/
HISAT2 v2.0.4	(Kim et al., 2015)	https://ccb.jhu.edu/software/hisat2/index.shtml
HTSeq v0.6.1	(Anders et al., 2015)	https://htseq.readthedocs.io/en/release_0.10.0/
Comet v2016.01 r3	https://doi.org/10.1002/pmic.201200439	v2016.01 r3
OpenSWATH v2.1.0	N/A	http://www.openswath.org/
MSstats v3.12.0	N/A	http://msstats.org/
Limma/voom	(Ritchie et al., 2015)/(Law et al.,2014)	https://bioconductor.org/packages/release/bioc/html/limma.html

(*Continued on next page*)

Continued

REAGENT or RESOURCE	SOURCE	IDENTIFIER
edgeR	(Robinson et al., 2010)	https://bioconductor.org/packages/release/bioc/html/edgeR.html
HiSeq control software HCS v3.4.0	Illumina	https://support.illumina.com/downloads/hiseq-x-hcs-v3-4-0.html
Bioconductor v3.5	Bioconductor	https://www.bioconductor.org/install/
GraphPad Prism v7.03	GraphPad Software, Inc.	https://www.graphpad.com/scientific-software/prism/
ImageJ	National Institutes of Health	https://imagej.nih.gov/ij/
Bruker TASQ software v2.1.22.3	Bruker	https://www.bruker.com/products/mass-spectrometry-and-separations/ms-software/tasq.html

LEAD CONTACT AND MATERIALS AVAILABILITY

This study did not generate new unique reagents. Further information and requests for resources and reagents should be directed to and will be fulfilled by the Lead Contact, Riekelt H. Houtkooper (r.h.houtkooper@amsterdamumc.nl).

EXPERIMENTAL MODEL AND SUBJECT DETAILS

Nematode Growing Conditions and RNAi Experiments

Worms were cultured at 20°C on nematode growth medium (NGM) agar plates seeded with OP50 strain *Escherichia coli*. In brief, synchronized N2 worms were harvested and snap frozen at L4 larval stage for either total mRNA isolation, polysome profiling, proteomics, or metabolomics. For RNAi knock down experiments, synchronized L1 worms were plated on NGMi (containing 2 mM IPTG) with a bacterial lawn of either *E. coli* HT115 (RNAi control strain, containing an empty vector) or *mrps-5, atf-5, eat-3*, *fzo-1, or skn-1* RNAi bacteria from the Ahringer *C. elegans* RNAi library. For double RNAi experiments bacteria were mixed in a 50/50 ratio and the control RNAi conditions were mixed with the empty vector (EV) RNAi bacteria HT115 in a 50/50 ratio. Lifespan tests were performed at 20°C as described (Houtkooper et al., 2013). In brief, synchronized worms were grown on NGM plates seeded with OP50 until reaching the L4 stage and then transferred to RNAi plates (F0). F0 adults were synchronized after 24h and transferred to NGMi RNAi plates to generate F1 offspring. At the L4 stage, F1 worms were transferred to plates containing 10 μM 5-Fluorouracil (5-FU, Sigma) to prevent growth of progeny. Worms were transferred to fresh RNAi plates once a week and after two transfers no 5-FU was added to plates.

K562 Cell Culture

K562 cells (female origin) were cultured at 37°C and in 5% CO_2 in antibiotic-free RPMI 1640 medium (Thermo Fischer Scientific) supplemented with 10% FBS (Bodinco) and 25 mM HEPES (VWR Life Science). After 48 treatment with either 20 μM amoxicillin (Sigma), 20 μM doxycycline (Sigma), or DMSO (Sigma) as a vehicle control (0.05% in media), cells were harvested for western blotting or polysome profiling.

C57BL/6J Germ-Free Mice

C57BL/6J germ-free male mice were housed 4 animals per cage and randomly assigned to the 3 experimental groups with N = 8 mice per treatment. The germ-free mice were housed in sterile flexible-film isolators (Getinge France, Les Ulis, France). They were given free access to autoclaved tap water and a gamma-irradiated (45 kGy) standard diet (R03; Scientific Animal Food and Engineering, Augy, France). The isolators were maintained at 20-24°C and on a 12-h light/dark cycle (lights on at 07:30am). The germ-free status was monitored weekly by microscopic examination and aerobic and anaerobic cultures of freshly voided feces. At the age of 9 weeks mice were treated for two weeks with either amoxicillin (50 mg/kg/d), or one of two doses of doxycycline (50 mg/kg/d or 500 mg/kg/d) in the drinking water supplemented with 5% sucrose. Mice were sacrificed after 12 hours of fasting, and the livers were harvested and snap frozen in liquid N_2. Liver tissue (~20 mg) was ground in liquid N_2 in a mortar and pestle and used for either mRNA isolation or polysome profiling. Procedures were carried out in accordance with the European guidelines for the care and use of laboratory animals; they were approved by the Ethics Committee of AgroParisTech and the INRA Research Center of Jouy-en-Josas (approval reference: 14–40).

METHOD DETAILS

BXD Strains

The BXD mouse liver proteome data used for network analyses were used from a prior publication (Williams et al., 2016) that consists of 73 cohorts of BXD mice—38 strains on chow diet and 35 strains on high fat diet for proteomics, and were combined. Note that the

raw liver proteomics data from PXD003266 from 2016 were re-analyzed using the newer SWATH search library from PXD005044 from 2018, which was designed to improve coverage for mitochondrial proteins. These re-processed and normalized and processed mouse data are also available as Table S1. BXD mouse multi-tissue data were used from a prior publication (Williams et al., 2018) using datasets available in the Gene Expression Omnibus (GEO; GSE60149, GSE60150, GSE60151, and GSE60489). BXD mouse liver proteome data for average abundance quantification (Figures 1C and 1D) were downloaded from www.genenetwork.org (GN540).

Network Analysis

Correlation network graphs were calculated using the above-referenced BXD proteome data using the iGraph v1.2.1 package in R. In the liver proteomics data, 77 cohorts were measured. 73 distinct cytosolic ribosome genes were quantified while 38 distinct mitochondrial ribosome genes were quantified. In the cross-tissue data, 40 samples from 5 tissues were measured. The cytosolic ribosome had 68 proteins quantified, while the mitochondrial ribosome had 55 proteins quantified. A fixed p value cutoff for both networks was used ($p < 5e\text{-}4$), with varying corresponding *rho* due to varying *n*. Note that protein expression is generally more highly variable across 40 samples from 5 tissues than it is across 77 samples just from liver. Nodes that have 0 or 1 edge connection to the rest of the network were visually suppressed, but are still counted in the edge and node counts reported. For significance testing, 10,000 random networks were permuted using the same input data and gene set size for each dataset and subset with gene sets of the same size selected at random out of the full proteomic datasets. A reported $p < 1e\text{-}4$ means that none of the 10,000 random networks were as significant as the selected ribosome gene sets taken from literature. Testing was only performed for overall edge counts.

Polysome Profiling

Gradients of 17%–50% sucrose (11 ml) in gradient buffer (110 mM KAc, 20 mM $MgAc_2$ and 10 mM HEPES pH 7.6) were prepared on the day before use in thin-walled, 13.2 mL polypropylene (14 × 89 mm) centrifuge tubes (Beckman-Coulter, USA). Approximately 5000 nematodes were lysed in 500 mL polysome lysis buffer (gradient buffer containing 100 mM KCl, 10 mM $MgCl_2$, 0.1% NP-40, 2 mM DTT, 0.5 mM cycloheximide and RNaseOUT (Thermo Fischer Scientific) using a Dounce homogenizer (Wheaton, USA) as described before (Molenaars et al., 2018). Mouse livers and K562 cells were lysed similarly with polysome lysis buffer but containing 5 mM cycloheximide. The samples were centrifuged at 1200 g for 10 min to remove debris and the supernatant was subjected to BCA protein assay (company). In all, 500 μg of total protein for each sample was loaded on top of the sucrose gradients. The gradients were ultra-centrifuged for 2 h at 40,000 *g* in a SW41Ti rotor (Beckman-Coulter, USA). The gradients were displaced into a UA6 absorbance reader (Teledyne ISCO, USA) using a syringe pump (Brandel, MD, USA) containing 60% sucrose. Absorbance was recorded at an OD of 254 nm. All steps of this assay were performed at 4°C or on ice and all chemicals came from Sigma-Aldrich (St. Louis, MO, USA) unless stated otherwise. Polysome peaks were quantified by measuring area under the curve (AUC) in ImageJ. Significance was tested with Student's t test, and p values were adjusted to correct for multiple testing using the Holm-Šídák method, with alpha = 0.05.

Seahorse Respirometry in C. elegans

Seahorse measurements were performed as described (Koopman et al., 2016). In brief, synchronized N2 worms grown on different RNAi conditions were collected at L4 larval stage, washed three times with M9 buffer, and ± 20 worms were transferred to 200 μl M9 buffer in a Seahorse XF96 microplate to measure respiration. Prior to and during the measurement the heater of the Seahorse respirometer was turned off. The chemical uncoupler FCCP (Abcam) and the complex IV inhibitor sodium azide (Sigma) treatments were used at a final concentration of 10 μM and 40 mM, respectively.

Metabolomics in C. elegans

A 75 μL mixture of the following internal standards in water was added to each freeze-dried sample: adenosine-$^{15}N_5$-monophosphate (100 μM), adenosine-$^{15}N_5$-triphosphate (1 mM), D_4-alanine (100 μM), D_7-arginine (100 μM), D_3-aspartic acid (100 μM), D_4-citric acid (100 μM), $^{13}C_1$-citrulline (100 μM), $^{13}C_6$-fructose-1,6-diphosphate (100 μM), guanosine-$^{15}N_5$-monophosphate (100 μM), guanosine-$^{15}N_5$-triphosphate (1 mM), $^{13}C_6$-glucose (1 mM), $^{13}C_6$-glucose-6-phosphate (100 μM), D_3-glutamic acid (100 μM), D_5-glutamine (100 μM), $^{13}C_6$-isoleucine (100 μM), D_3-leucine (100 μM), D_4-lysine (100 μM), D_3-methionine (100 μM), D_6-ornithine (100 μM), D_5-phenylalanine (100 μM), D_7-proline (100 μM), $^{13}C_3$-pyruvate (100 μM), D_3-serine (100 μM), D_5-tryptophan (100 μM), D_4-tyrosine (100 μM), D_8-valine (100 μM). Subsequently, 425 μL water, 500 μL methanol was added and worms were homogenized with a 5 mm steel bead using a TissueLyser II (QIAGEN) for 5 min at frequency of 30 times/sec, and 1 mL chloroform was added to the same 2 mL tube before thorough mixing and centrifugation for 10 min at 14.000 rpm. The top layer, containing the polar phase, was transferred to a new 1.5 mL tube and dried using a vacuum concentrator at 60°C. Dried samples were reconstituted in 100 μL methanol/water (6/4; v/v). Metabolites were analyzed using a Waters Acquity ultra-high performance liquid chromatography system coupled to a Bruker Impact II Ultra-High Resolution Qq-Time-Of-Flight mass spectrometer. Samples were kept at 15°C during analysis and 5 μL of each sample was injected. Chromatographic separation was achieved using a Merck Millipore SeQuant ZIC-cHILIC column (PEEK 100 × 2.1 mm, 3 μm particle size). Column temperature was held at 30°C. Mobile phase consisted of (A) 1:9 acetonitrile:water and (B) 9:1 acetonitrile:water, both containing 5 mM ammonium acetate. Using a flow rate of 0.25 mL/min, the LC gradient consisted of: 100% B for 0-2 min, ramp to 0% B at 28 min, 0% B for 28-30 min, ramp to 100% B at 31 min, 100% B for 31-35 min. MS data were acquired using negative ionization in full scan mode over the range of m/z 50-1200. Data were analyzed using Bruker TASQ software version 2.1.22.3. All reported metabolite intensities were normalized to the number of worms in each

sample, as well as to internal standards with comparable retention times and response in the MS. Metabolite identification has been based on a combination of accurate mass, (relative) retention times and fragmentation spectra, compared to the analysis of a library of standards.

Western Blotting

For extraction of protein, K562 pellets were resuspended in RIPA buffer with cOmplete Mini Protease Inhibitor Cocktail (Sigma-Aldrich). Lysates were incubated on ice for 10 min and then centrifuged at 16,000 x g for 10 min in a pre-chilled centrifuge to remove debris and quantification was carried out with BCA protein assay. Equal amounts of protein (25-50 μg) were loaded onto NuPAGE® Novex 4%–12% Bis-Tris Gel 1.5 mm, 10 Well (Invitrogen) and subsequently transferred to nitrocellulose membranes using iBlot 2 Transfer Stacks (Invitrogen) for 7 min at 14 V in iBlot 2 Dry Blotting System (Invitrogen). Western blotting was performed with antibodies against ATF4 (Cell Signaling Technology, #11815), β-actin (Sigma-Aldrich, #A5441), IRDye® 680RD Donkey anti-Rabbit secondary antibody (Li-Cor, #925-68073), and IRDye® 800CW Goat anti-Mouse secondary antibody (Li-Cor, #925-32210) and visualized using the Odyssey® Imaging System.

Isolation of mRNA (Total, Monosomal, and Polysomal)

For isolation of total mRNA, whole worms or liver tissue were homogenized with a 5 mm steel bead using a TissueLyser II (QIAGEN) for 5 min at frequency of 30 times/sec in the presence of TRIzol (Invitrogen), then the isolation was continued according to manufacturer's protocol. Polysomal or monosomal fractions from two experiments were pooled and mRNA was extracted using TRIzol Liquid Sample (LS) (Invitrogen) according to the manufacturer's protocol. For RNaseq, contaminating genomic DNA was removed using RNase-Free DNase (QIAGEN) and samples were cleaned up with the RNeasy MinElute Cleanup Kit (QIAGEN).

Library Preparation

RNA libraries were prepared and sequenced with the Illumina platform by Genome Scan (Leiden, Netherlands). Libraries were prepared using the NEBNext Ultra Directional RNA Library Prep Kit (NEB #E7420) according to manufacturer's protocols. Briefly, rRNA was depleted from total RNA using the rRNA depletion kit (NEB# E6310). After fragmentation of the rRNA-reduced RNA, a cDNA synthesis was performed in order to ligate with the sequencing adapters and PCR amplification of the resulting product. Quality and yields after sample preparation were measured with the Fragment Analyzer (Agilent). Sizes of the resulting products were consistent with the expected size distribution (a broad peak between 300-500 bp). Clustering and DNA sequencing using the Illumina cBot and HiSeq 4000 was performed according to manufacturer's protocol with a concentration of 3.0 nM of DNA. HiSeq control software HCS v3.4.0, image analysis, base calling, and quality check was performed with the Illumina data analysis pipeline RTA v2.7.7 and Bcl2fastq v2.17.

Read Mapping, Statistical Analyses, and Data Visualization

Reads were subjected to quality control FastQC (Andrews, 2010) trimmed using Trimmomatic v0.32 (Bolger et al., 2014) and aligned to either the *C. elegans* (worm) or *M. musculus* (mouse) genomes obtained from Ensembl, wbcel235.v91 and GRCm38v87, respectively, using HISAT2 v2.0.4 (Kim et al., 2015). Worm and mouse samples were analyzed separately; different fractions (total, monosomal, polysomal) within each species were analyzed together. Counts were obtained using HTSeq (v0.6.1, default parameters) (Anders et al., 2015) using the corresponding GTF taking into account the directions of the reads. Statistical analyses were performed using the edgeR (Robinson et al., 2010) and limma/voom (Ritchie et al., 2015) R packages. All genes with more than 2 counts in at least 4 of the samples were kept. Count data were transformed to log2-counts per million (logCPM), normalized by applying the trimmed mean of M-values method (Robinson et al., 2010) and precision weighted using voom (Law et al., 2014). All data analyses and visualizations were done using transcript data with a count value greater than 0. Differential expression was assessed using either an empirical Bayes moderated t test within limma's linear model framework including the precision weights estimated by voom (Ritchie et al., 2015; Law et al., 2014), or a Partial least-squares discriminant analysis (PLS-DA) using mixomics (Rohart et al., 2017) setting a variable of importance (VIP) score of greater than 1 as significant. Resulting *p* values (where applicable) were corrected for multiple testing using the Benjamini-Hochberg false discovery rate. Genes were re-annotated using biomaRt using the Ensembl genome databases (v91). Data visualization was performed using gplots (Warnes et al., 2016) and ggplot2 (Wickham, 2009) selecting colors from RcolorBrewer (Neuwirth, 2014). Data processing and visualization was performed using R v3.4.3 and Bioconductor v3.5. The RNA-seq data are available on GEO under the ID GSE122097.

Translational Efficiency Calculations

Translational efficiencies (TEs) were acquired by considering the ratio of a highly translated ribosome-mRNA fraction (i.e., polysomal RNA) over a lower translated ribosome-mRNA fraction (i.e., either monosomal RNA for C. *elegans* or total RNA for *M. musculus*). Monosomal RNA was used for *C. elegans* as it showed an increase in abundance in our polysome profiles. The monosomal fraction did not show an increase in abundance in *M. musculus* and therefore total RNA was used. This ratio (highly translated ribosome-mRNA fraction / lower translated ribosome-mRNA fraction) was then compared between treated samples (i.e., *mrps-5* for *C. elegans* or doxycycline treatment for *M. musculus*) and control samples (i.e., empty vector for *C. elegans* or Amoxicilin treatment for *M. musculus*). This resulted in TE being defined as: $\log2[(\text{treated}^{\text{polysome}} / \text{treated}^{\text{monosome}}) / (\text{control}^{\text{polysome}} / \text{control}^{\text{monosome}})]$ in the case of *C. elegans* and $\log2[(\text{treated}^{\text{polysome}} / \text{treated}^{\text{total}}) / (\text{control}^{\text{polysome}} / \text{control}^{\text{total}})]$ in the case of *M. musculus*. Means from each set of replicates were used to calculate the ratios. A TE value was defined as significant if the gene in question had a PLS-DA VIP

score above 1, in either the polysomal RNA (for both *C. elegans* and *M. musculus*) or monosomal RNA (for *C. elegans*) or total RNA (for *M. musculus*), and changed at least 1.25 fold in its TE (to eliminate noise of near zero TEs).

Reverse Transcription and qPCR

For qPRC, 1 μg of extracted RNA was pre-treated with gDNA Wipeout Buffer and reverse transcribed into cDNA according to the manufacturer's instructions using the QuantiTect Reverse Transcription Kit (QIAGEN). Quantitative gene expression analysis was performed using the LightCycler® 480 SYBR Green I Master (Roche) and measured using the LightCycler® 480 Instrument (Roche). Relative expression was calculated with the linRegPCR method ((Ruijter et al., 2009) and normalized to reference genes (*F35G12.2* and *pmp-3*). A complete list of primers is available in Key Resources Table.

Protein-Transcript Cross Comparison

Fold change (log2 transformed) of the genes in common between the transcriptome and proteome data were plotted in a co-regulation plot, with mRNA or protein data on the X or y axis, respectively. A cutoff was used to eliminate noise of near zero-fold change when identifying genes differentially expressed in the plot. Selecting cutoffs relative to each dataset allowed us to address the large difference in fold changes observed between the different mRNA and protein datasets, and we therefore used a quarter of the standard deviation of each log2-transformed dataset's distribution as a standard threshold for noise (dashed line in plot). This corresponded to a value of 1.13 (0.179 in log2 scale) for the transcriptome and 1.01 (0.016 in log2 scale) for the proteome. Values above these cutoffs in each respective dataset that had VIP scores above 1 were considered as significant in the quadrants of the co-regulation plot.

Worm-Mouse Cross Comparison

Worm and mouse orthologous genes were acquired using the R package annotationTools (Kuhn et al., 2008) and HomoloGene v68 species annotation.

Ribosomal Gene Lists

Cytosolic and mitochondrial ribosomal gene lists for both *C. elegans* and *M. musculus* were downloaded from the Ribosomal Protein Gene Database (http://ribosome.med.miyazaki-u.ac.jp/).

Functional Annotation of Gene Sets

Gene sets were analyzed for functional enrichments using the DAVID bioinformatics resource version 6.8 (Huang da et al., 2009). Functional annotation clustering was performed using DAVID defined default settings incorporating gene sets from Gene Ontologies (biological process, cellular component, and molecular function), functional categories (including Clusters of Orthologous Groups (COG) ontologies, UP keywords, UP seq features), pathways (including KEGG), and protein domains (including INTERPRO PIR superfamily and SMART). Background datasets to check enrichments against included the measured transcriptome (for enrichments at mRNA level within a single species), measured proteome (for enrichments at the protein level), gene overlap between the measured transcriptome and proteome (for enrichments of the co-regulation analysis), or genes in common between mouse and worms (for cross-species enrichment). Resulting clusters were manually annotated for purposes of visualization and summarization. Clusters with an 'Enrichment Score' above 1.3 ($p < 0.05$) were considered significantly enriched.

Protein Isolation for SWATH Proteomics

Worm pellets were freeze-dried overnight and stored at room temperature until use. *C. elegans* proteins were isolated using the standard protocol used for tissue preparation (Wu et al., 2017) with the exception that, to ensure that the cuticle was fully ruptured, during the protein isolation from total cells in 8M urea, the samples were sonicated at a high power (150 W) for 10x10 cycles of 10 s (UP200St-G sonicator, Hielsher, Germany). In brief (see above source for more details): proteins were extracted in an 8M urea buffer, 300 μg were aliquoted and precipitated by acetone overnight, then reduced with DTT, alkylated with IAA, and digested with trypsin at a 1:25 ratio. C18 spin columns (The Nest Group) were used for cleanup.

SWATH Proteomics – Library Acquisition

For library acquisition, 150 μg of digested peptide from three sets of pooled N2 wild-type adult *C. elegans* were pH fractionated (protocol #84868, Thermo Fisher Scientific) into 10 fractions. The resulting 30 fractions were separated on an Eksigent liquid chromatography machine coupled with a 20 cm PicoFrit emitter injected on an AbSciex 5600+ TripleTOF using a 120 min gradient going from 2% to 35% acetonitrile at 300 nL/minute. At the MS1 level, the 20 most intense precursors were selected in the range of 350 – 1460 m/z with a 500 ms survey scan. At the MS2 level, spectra were acquired at 150 ms survey scans between 50 - 2000 m/z. These samples were used for preparing a spectral library to support the DIA/SWATH data (Röst et al., 2014). iRT peptides (Biognosys) were added to all samples, for both DDA injections (library acquisition) and DIA injections (for quantification).

SWATH Proteomics – Sample Acquisition

For all samples measured for quantitative DIA (SWATH) acquisition, 1 μg of non-fractionated sample were injected in the same AbSciex 5600+ TripleTOF using the same parameters except using a 60 min gradient and in data-independent acquisition mode using 64 m/z windows. The output .wiff files from both DIA and DDA acquisition mode were converted to centroided mzXML files using FileConverter v2.2.0. For library generation from the DDA mzXML files, samples were searched against the canonical UniProtKB *C. elegans* proteome database containing 27481 proteins and searched with Comet v2016.01 r3. Reverse decoy proteins were generated and up to 2 tryptic missed cleavages were allowed with a precursor mass error of 50 ppm and fragment error of 0.1 Da. Cysteine carbamidomethylation was used as the fixed modification and methionine oxidation as the variable modification. PeptideProphet was used to search the data and scored with iProphet. A 1% protein FDR was used for significance cutoff.

The in-house results from the DDA runs were combined with extensive published *C. elegans* DDA data (PXD004584) and (Narayan et al., 2016). The light channel from these SILAC-labeled samples was also searched with Comet as above, using the same parameters, using CiRT peptides instead of iRT peptides (Parker et al., 2015). The results from the in-house and downloaded DDA files were combined, and peptides with retention time variance of $\geq$ 150 were removed. For peptides identified in-house and in the downloaded dataset, the in-house peptide was retained and the other peptide discarded. The final assembled library contains 67'612 peptides (of which 18'072 from the in-house DDA runs and 49'540 from the downloaded DDA runs), corresponding to 9'438 unique proteins. This library was then used as the reference library for OpenSWATH v2.1.0. OpenSWATH was run on all DIA acquisitions, followed by mProphet scoring using the msproteomicstools package available on GitHub (September 2017). 10750 peptides corresponding to 1715 proteotypic proteins were quantified. Protein data were generated from the peptide matrix using MSstats v3.12.0. Differential expression was determined using either a Student's t test (with *p* values corrected for multiple testing using the Benjamini-Hochberg false discovery rate, presented for reference) or partial least-squares discriminant analysis (PLS-DA) with mixomics (Rohart et al., 2017) setting a variable of importance (VIP) score of greater than 1 as significant. The DIA data and the assembled library file are available on PRIDE under the ID PXD009223.

QUANTIFICATION AND STATISTICAL ANALYSIS

Statistical details and tests used, the number and representation of n and any other forms of quantification present are specified in the respective figure legends and results section. Statistical analyses for quantified polysome profiles and western blotting (WB) were performed using the Prism 7 software (GraphPad Software, La Jolla, CA, USA). Significance was tested with Student's t test, and *p-value*s were adjusted to correct for multiple testing using the Holm-Šídák method. All other statistics were performed as described in each respective methods section and unless otherwise noted, were performed using R v3.4.3. Gene expression was considered differential relative to control using the variable of importance (VIP) score from a partial least-squares discriminant analysis (PLSA-DA) greater than 1. In all supplemental tables where relevant, *p-value*s (Bayes moderated t test for transcriptomics or Student's t test for proteomics), and adjusted *p-value*s (Benjamini-Hochberg method) are presented in addition to the VIP scores (from PLS-DA). For lifespan studies, survival curves were calculated using the log-rank (Mantel-Cox) method.

DATA AND CODE AVAILABILITY

The accession number for the *C. elegans* and mice RNA sequencing data reported in this paper is GEO: GSE122097. The proteomics DIA data and the assembled library file are available on PRIDE under the ID PXD009223. The reference liver mouse transcriptomics and proteomics data examined in Figure 1 are available under GEO at GSE60149 and PRIDE at PXD003266. The reference multi-tissue mouse transcriptome data are available under GEO GSE60149, GSE60150, GSE60151, and GSE60489 and are from the same mice despite the non-continuous and separate entries. The multi-tissue proteomics data are from PXD005044. Note that the raw liver proteomics data from PXD003266 from 2016 were re-analyzed using the newer SWATH search library from PXD005044 from 2018, which was designed to improve coverage for mitochondrial proteins. These re-processed and normalized and processed mouse data are also available as Table S1.